

Air Force Institute of Technology

AFIT Scholar

Theses and Dissertations

Student Graduate Works

12-1997

The Fate and Transport of Airborne JP-4 and JP-8 Aerosol During Cold Startup

Bradford Eugene Buckman

Follow this and additional works at: <https://scholar.afit.edu/etd>



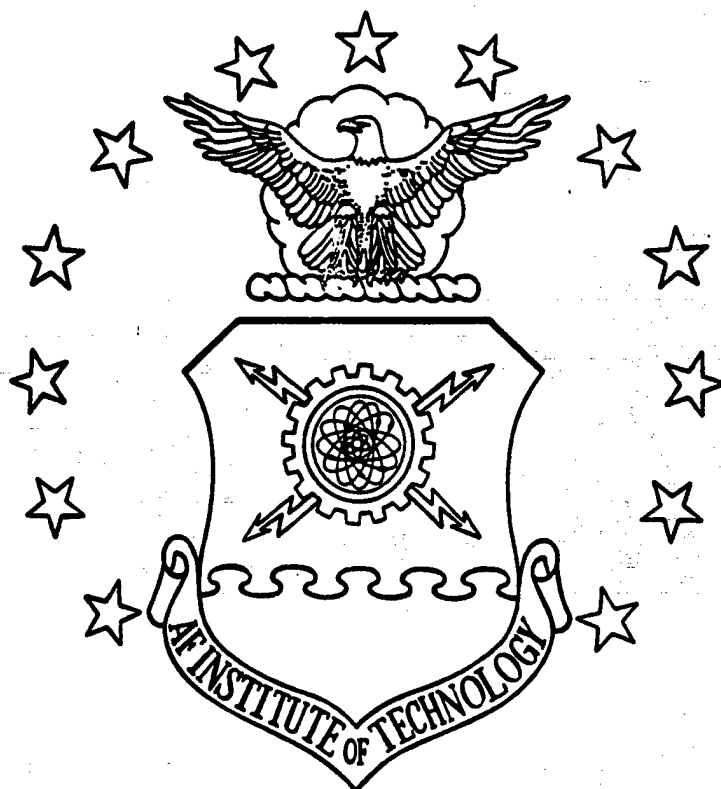
Part of the [Applied Mathematics Commons](#), and the [Environmental Monitoring Commons](#)

Recommended Citation

Buckman, Bradford Eugene, "The Fate and Transport of Airborne JP-4 and JP-8 Aerosol During Cold Startup" (1997). *Theses and Dissertations*. 5589.

<https://scholar.afit.edu/etd/5589>

This Thesis is brought to you for free and open access by the Student Graduate Works at AFIT Scholar. It has been accepted for inclusion in Theses and Dissertations by an authorized administrator of AFIT Scholar. For more information, please contact AFIT.ENWL.Repository@us.af.mil.



**The Fate and Transport of Airborne JP-4
and JP-8 Aerosol During Cold Startup**

THESIS
Bradford Eugene Buckman
Captain, USAF

AFIT/GEE/ENC/97D-02

DISTRIBUTION STATEMENT A

**Approved for public release;
Distribution Unlimited**

DTIC QUALITY INSPECTED 8

DEPARTMENT OF THE AIR FORCE
AIR UNIVERSITY
AIR FORCE INSTITUTE OF TECHNOLOGY

Wright-Patterson Air Force Base, Ohio

19980114 126

**The Fate and Transport of Airborne JP-4
and JP-8 Aerosol During Cold Startup**

**THESIS
Bradford Eugene Buckman
Captain, USAF**

AFIT/GEE/ENC/97D-02

DTIC QUALITY INSPECTED 3

The Fate and Transport of Airborne JP-4 and JP-8 Aerosol During Cold Startup

THESIS

Bradford Eugene Buckman

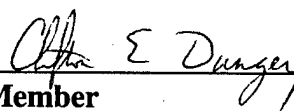
Presented to the Faculty of the School of Engineering

of the Air Force Institute of Technology

In Partial Fulfillment of the

Requirements for the Degree of

Master of Science in Engineering and Environmental Management


Member


Member


Chairman

Acknowledgments

I am very grateful to the good advise and time spent with my thesis advisor, Dr. Dennis Quinn. He showed a lot of patience and kept me on the right course as we progressed through the thesis journey.

I also want to thank the members of the thesis committee, Maj. Cliff Dungey and Maj. Jim Aldrich. Their instruction in class and insights during the thesis process were essential in the overall production of the thesis, for which I am also very grateful.

I also wish to thank other members of the AFIT faculty who either facilitated my overall understanding of the problem at hand, and/or taught the tools necessary to analyze and present the topic. Most notable in this area were Lt. Col. Glen Perram and Dr. Dan Reynolds.

Finally, I wish to thank the AFIT Technical Library for providing the material and support needed to complete the research, and ENV secretary Ida Carruthers for her support and patience.

Bradford Eugene Buckman

Table of Contents

	Page
Acknowledgments.....	ii
List of Figures.....	vi
List of Tables.....	viii
Abstract.....	ix
I. Introduction.....	1-1
1.1 Overview	1-1
1.2 Problem.....	1-2
1.3 Hypothesis.....	1-2
1.4 Scope.....	1-3
1.5 Approach.....	1-4
1.6 Limitations of Underlying Assumptions.....	1-4
1.7 Summary of Thesis.....	1-5
II. Background	
2.1 Overview.....	2-1
2.2 Lowell, 1959.....	2-1
2.3 Fuchs, 1964.....	2-2
2.4 Friedlander, 1977.....	2-3
2.5 Clewell, 1983.....	2-4
2.6 Finlayson-Pitts & Pitts, 1986.....	2-5
2.7 Seinfeld, 1986.....	2-7

2.8 Summary.....	2-9
III. Methodology.....	3-1
3.1 Overview.....	3-1
3.2 Initial Conditions.....	3-1
3.2.1 Plume Composition.....	3-1
3.2.2 Plume Geometry.....	3-2
3.2.3 Plume Diameter Distribution.....	3-2
3.3 Plume Settling.....	3-3
3.3.1 Method of Settling.....	3-3
3.3.2 Stokes' Formula.....	3-4
3.4 Plume Advection and Dispersion.....	3-5
3.4.1 The Atmospheric Diffusion Equation.....	3-5
3.4.2 Advection.....	3-6
3.4.3 Dispersion.....	3-6
3.4.4 Gaussian Solution to Atmospheric Diffusion Equation.....	3-7
3.5 Evaporation.....	3-8
3.5.1 Assumptions.....	3-8
3.5.2 Evaporation Formula.....	3-9
3.5.3 Design Considerations.....	3-10
3.6 Numerical Methods.....	3-11
3.6.1 Lagrangian Assumption.....	3-11
3.6.2 Solution of the Diffusion Equation.....	3-11
3.6.3 The 3-D Case.....	3-12
3.7 Summary.....	3-12
III. Model Results.....	4-1
4.1 Overview.....	4-1
4.2 Aerosol Settling.....	4-1

4.2.1 Count Versus Mass Distribution.....	4-1
4.2.2 Time to Ground of the Aerosol.....	4-2
4.3 Aerosol Advection and Dispersion.....	4-6
4.3.1 Assumption of Point Source.....	4-6
4.3.2 Atmospheric Variation.....	4-6
4.3.3 Continuous Source.....	4-7
4.3.4 Instantaneous Source.....	4-11
4.3.5 Summary of Advection-Dispersion Results.....	4-16
4.4 Evaporation and Settling Combined.....	4-17
4.4.1 Evaporation of JP-4 Droplets.....	4-17
4.4.2 Evaporation of JP-8 Droplets.....	4-25
4.4.3 JP-4 and JP-8 Constituents.....	4-30
4.4.4 Total Evaporation With Time of JP-4 and JP-8.....	4-34
4.4.5 Determination of Accurate Source Terms.....	4-37
4.5 Combined Settling / Advection / Dispersion / Evaporation of JP-4 and JP-8.....	4-38
4.6 Summary of Results.....	4-48
V. Conclusion.....	5-1
5.1 Summary.....	5-1
5.1.1 Aerosol Settling.....	5-1
5.1.2 Aerosol Advection and Dispersion.....	5-1
5.1.3 Aerosol Evaporation.....	5-1
5.2 Conclusions.....	5-2
5.3 Recommendations.....	5-3
Appendix A. Evaporation Model.....	A-1
Appendix B. Clewell's Fuel Component Models.....	B-1
Bibliography.....	BIB-1
Vita.....	Vita-1

List of Figures

Figure	Page
4.1 Comparison of Count Distribution Versus Mass Distribution of Particles.....	4-2
4.2 Diameter Versus Settling Velocity.....	4-4
4.3 Diameter Versus Time To Reach Ground.....	4-5
4.4 Time Versus Percentage of Mass Left.....	4-5
4.5 Distance vs. Max Downwind Concentration, Case A-B, Continuous Case.....	4-8
4.6 Distance vs. Max Downwind Concentration, Case B-C, Continuous Case.....	4-9
4.7 Distance vs. Max Downwind Concentration, Case C-D, Continuous Case.....	4-10
4.8 Distance vs. Max Downwind Concentration, Case A-B, Instantaneous Case.....	4-12
4.9 Distance vs. Max Downwind Concentration, Case B-C, Instantaneous Case.....	4-14
4.10 Distance vs. Max Downwind Concentration, Case C-D, Instantaneous Case....	4-15
4.11 Evaporation of 7.5 μm JP-4 Droplet.....	4-18
4.12 Evaporation of 15 μm JP-4 Droplet.....	4-19
4.13 Evaporation of 25 μm JP-4 Droplet.....	4-20
4.14 Evaporation of 35 μm JP-4 Droplet.....	4-21
4.15 Evaporation of 45 μm JP-4 Droplet.....	4-21
4.16 Evaporation of 55 μm JP-4 Droplet.....	4-22
4.17 Evaporation of 65 μm JP-4 Droplet.....	4-22
4.18 Evaporation of 75 μm JP-4 Droplet.....	4-22
4.19 Evaporation of 85 μm JP-4 Droplet.....	4-23
4.20 Evaporation of 95 μm JP-4 Droplet.....	4-23
4.21 Evaporation of 105 μm JP-4 Droplet.....	4-23
4.22 Evaporation of 115 μm JP-4 Droplet.....	4-24
4.23 Evaporation of 7.5 μm JP-8 Droplet.....	4-26
4.24 Evaporation of 15 μm JP-8 Droplet.....	4-26
4.25 Evaporation of 25 μm JP-8 Droplet.....	4-27
4.26 Evaporation of 35 μm JP-8 Droplet.....	4-27
4.27 Evaporation of 45 μm JP-8 Droplet.....	4-27
4.28 Evaporation of 55 μm JP-8 Droplet.....	4-28
4.29 Evaporation of 65 μm JP-8 Droplet.....	4-28
4.30 Evaporation of JP-4 Constituents C6-C9, OC and 35 μm	4-31
4.31 Evaporation of JP-4 Constituents C10-C14, OC and 35 μm	4-31
4.32 Evaporation of JP-8 Constituents C6-C9, OC and 35 μm	4-32
4.33 Evaporation of JP-8 Constituents C10-C14, OC and 35 μm	4-33
4.34 JP-4 Evaporation/Dispersion at -20°C, Continuous Case (A-B).....	4-39
4.35 JP-4 Evaporation/Dispersion at -20°C, Instantaneous Case (A-B).....	4-40
4.36 JP-4 Evaporation/Dispersion at 0°C, Continuous Case (A-B).....	4-40
4.37 JP-4 Evaporation/Dispersion at 0°C, Instantaneous Case (A-B).....	4-40
4.38 JP-4 Evaporation/Dispersion at 20°C, Continuous Case (A-B).....	4-41
4.39 JP-4 Evaporation/Dispersion at 20°C, Instantaneous Case (A-B).....	4-41
4.40 JP-8 Evaporation/Dispersion at -20°C, Continuous Case (A-B).....	4-41

4.41 JP-8 Evaporation/Dispersion at -20°C, Instantaneous Case (A-B).....	4-42
4.42 JP-8 Evaporation/Dispersion at 0°C, Continuous Case (A-B).....	4-42
4.43 JP-8 Evaporation/Dispersion at 0°C, Continuous Case (A-B).....	4-42
4.44 JP-8 Evaporation/Dispersion at 20°C, Continuous Case (A-B).....	4-43
4.45 JP-8 Evaporation/Dispersion at 20°C, Continuous Case (A-B).....	4-43

List of Tables

Table	Page
4.1 Comparison of Diameter, Mass, Settling Velocity and Time.....	4-3
4.2 Values of Time vs. Percentage of Mass Left of the Airborne Aerosol.....	4-5
4.3 Concentration in the +/- Y Direction, Case A-B, Continuous Case.....	4-8
4.4 Concentration in the +/- Y Direction, Case B-C, Continuous Case.....	4-10
4.5 Concentration in the +/- Y Direction, Case C-D, Continuous Case.....	4-11
4.6 Concentration in the +/- Y Direction, Case A-B, Instantaneous Case.....	4-13
4.7 Concentration in the +/- Y Direction, Case B-C, Instantaneous Case.....	4-14
4.8 Concentration in the +/- Y Direction, Case C-D, Instantaneous Case.....	4-15
4.9 Critical Distances for Three Different Engine Types.....	4-16
4.10 Mass Remaining at Various Times for JP-4 Droplets.....	4-19
4.11 Amount of JP-4 Reaching Ground.....	4-25
4.12 JP-8 Evaporation Cases for Various Temperatures.....	4-29
4.13 Amount of JP-8 Reaching Ground.....	4-29
4.14 JP-4 Constituents (Remaining Proportions) at 0°C for 35 μm	4-32
4.15 JP-4 Constituents (Remaining Proportions) at 0°C for 35 μm	4-33
4.16 Evaporation of JP-4 at -20°C.....	4-34
4.17 Evaporation of JP-8 at -20°C.....	4-35
4.18 Evaporation of JP-4 at 0°C.....	4-35
4.19 Evaporation of JP-8 at 0°C.....	4-36
4.20 Evaporation of JP-4 at 20°C.....	4-36
4.21 Evaporation of JP-8 at 20°C.....	4-37
4.22 Determination of the Source Term for JP-4 and JP-8 at 0°C.....	4-38
4.23 Concentration ($\mu\text{g}/\text{m}^3$) Versus Time for JP-4 at -20°C.....	4-44
4.24 Concentration ($\mu\text{g}/\text{m}^3$) Versus Time for JP-4 at 0°C.....	4-45
4.25 Concentration ($\mu\text{g}/\text{m}^3$) Versus Time for JP-4 at 20°C.....	4-45
4.26 Concentration ($\mu\text{g}/\text{m}^3$) Versus Time for JP-8 at -20°C.....	4-46
4.27 Concentration ($\mu\text{g}/\text{m}^3$) Versus Time for JP-8 at 0°C.....	4-46
4.28 Concentration ($\mu\text{g}/\text{m}^3$) Versus Time for JP-8 at 20°C.....	4-47
4.29 Critical Time and Distances for Various Conditions, Continuous Case.....	4-47
4.30 Critical Time and Distances for Various Conditions, Instantaneous Case.....	4-48

Abstract

During cold startup (engine warm-up) procedures at northern tier bases, fuel aerosol (JP-4 and JP-8) is emitted before complete combustion of the fuel occurs. The time necessary for complete combustion to occur may be as long as 10 minutes. Hence, during these first few minutes, aerosol is emitted at relatively high concentrations. This research investigates the principle behavior of the emitted aerosol: advection, dispersion, evaporation, and settling. Using previous work in fuel jettisoning and evaporation as a foundation, this thesis investigates the physical factors affecting the airborne concentration of fuel aerosol at different times, the amount of fuel aerosol reaching the ground, and the times and distances necessary for the aerosol concentration to fall below the hydrocarbon standard after being emitted. Physical assumptions in the model are presented, and various atmospheric conditions are simulated for comparison.

The Fate and Transport of Airborne JP-4 and JP-8 Aerosol During Cold Startup

I. Introduction

1.1 Overview.

During cold startups at northern tier Air Force Bases, the fuel aerosol (JP-4 and JP-8) in an aircraft engine is emitted at very high concentrations due to little or no combustion during the first 5-10 minutes of the process. These procedures are necessary for engine warm-up, and the fuel that is consequently emitted has an initially high airborne concentration. While sedimentation will cause much of the airborne aerosol to fall to the ground quickly, the smaller aerosol may remain airborne at significant concentrations for longer times.

Dispersion aerosols are formed by the grinding or atomization of solids and liquids by the transfer of powders into a state of suspension through the action of air currents or vibration. The first authoritative work on the mechanics of aerosols was compiled by Fuchs (10) in 1964, in which he discussed the important mechanisms of aerosol formation, growth, and motion. His work, however, was incomplete in the areas of coagulation and precipitation of aerosols in turbulent flow. Subsequent works and studies by Friedlander (9), Seinfeld (24) and others then further enhanced the understanding of aerosol mechanics, building on the work of Fuchs.

Previous work developed by Lowell (17, 18), Clewell (4, 5) and others have investigated the fate of fuel jettisoned at various altitudes and airspeeds. This effort is intended to apply the previously studied processes of evaporation, advection, and dispersion of jettisoned jet fuel to the problem at hand. Ultimately, we are interested in

the affects of inhaling aerosol pollutants: "Aerosols may affect human health...particle size, concentration, and chemical composition are usually the most important factors..." (9:3).

1.2 Problem.

Because of the high concentrations being emitted into the environment at ground level, workers may be exposed to unusually high concentrations of airborne fuel aerosol. In addition, much of this initially airborne aerosol will fall to the ground due to sink mechanisms (namely sedimentation) and subsequently may seep into the groundwater. With the human health implications, it is the intent of this preliminary study to characterize the fuel aerosol size distribution, concentration, and chemical constituent breakdown at different times and atmospheric conditions.

1.3 Hypothesis.

This study is based on the hypothesis that the majority of the mass of particles in the aerosol will settle out and hit the ground relatively quickly due to sedimentation. In addition, the remaining airborne particles will also eventually be removed from the atmosphere at later times due to Brownian (thermal) motion and various sink mechanisms (such as dry deposition and washout). Friedlander found that: "...very small particles (in an aerosol) are removed by Brownian motion, whereas the larger ones settle out or deposit because their inertia does not permit them to follow the turns in the air flow." (9:3).

Therefore, if the amount of airborne particles is constantly changing due to various physical processes, the concentration of airborne fuel aerosol is also constantly changing and this phenomena must be investigated.

1.4 Scope.

This research covers three basic questions of concern: what is the particle size distribution of JP-4 or JP-8 aerosol emitted during cold-startup at a northern tier base, what is the concentration of the airborne aerosol at various times, and what is the chemical constituent breakdown of the aerosol at these various times.

1. Particle size distribution. The particle size distribution is described by the log-normal probability distribution, and is assumed to be constant with time (neglecting coagulation and condensation).
2. Mass Concentration of Aerosol. The primary factors affecting the mass concentration of an aerosol are the source term (dependent on the aircraft), and the atmospheric conditions; K-theory advection and dispersion will model the rate of change of the concentration as a function of the source term, time, and atmospheric conditions.
3. Chemical Constituent Breakdown. The evaporation model will describe the rate of change of the various chemical constituents of JP-4 and JP-8, and evaporation will be dependent on atmospheric conditions.

1.5 Approach.

We must create a model for predicting the three phenomena of concern. Again, the approach will be divided into the three analytical parts described in the scope.

1. We must first determine a way to quantify the parameters of the particle size distribution (mean and standard deviation). This will be accomplished by determining the maximum and minimum extremes of particle sizes for the mist we are analyzing and fitting a log-normal distribution to this range.
2. For the second part of our study, we will model downwind aerosol concentrations as function of the source term, atmospheric conditions, and time. This will require advection and dispersion analysis of the airborne aerosol with time.
3. For the third part of our study, we will model the evaporation of the various chemical constituents and total evaporation of the JP-4 and JP-8 aerosol by using Law's analysis to describe the governing equations for the multi-component evaporation model (21:1), as well and making use of the previous work with jettisoned jet fuel.

1.6 Limitations of Underlying Assumptions.

The following are some simplifying assumptions that represent limitations to this study:

1. *Turbulence.* The turbulence that is created from the engine exhaust is neglected for the scope of this study. It is assumed that wind is the primary transport

mechanism upon emission of the fuel from the engine. This will inherently give more conservative results in terms of airborne concentrations of the aerosol.

2. *Cold Startup Time.* It is assumed that the duration of the cold startup process is ten minutes, regardless of the ambient temperature. However, temperature would indeed affect the cold startup times; a higher ambient temperature would likely decrease the time of the engine to warm-up and combust the fuel efficiently.
3. *Vapor.* The concentrations of JP-4 and JP-8 vapor are not a part of this study. Once the aerosol is evaporated and becomes vapor, it is neglected; however, the concentrations of the remaining vapor are indeed important for air pollution and inhalation studies, which are beyond the scope of this study. The airborne hydrocarbon standard of $160 \mu\text{m}^3$ (29:51) is for hydrocarbon vapor, but is used in this study as an aerosol concentration for purposes of comparisons across different stability classes, fuel types, and temperature. It is not the intent of this study to make conclusions regarding potential health effects of the airborne aerosol and/or the airborne vapor.
4. *Particle Size Distribution.* The aerosol particle size distribution will change with time due to the effects of coagulation and condensation in the aerosol. We neglect these effects and assume a constant particle size distribution with time.

1.7 Summary of Thesis.

The thesis is organized as follows:

Chapter II reviews background material in the field of aerosol mechanics and air pollution transport, as well as aerosol evaporation studies.

Chapter III presents the methodology with which we develop our model.

Chapter IV presents results from each of our model considerations: settling, advection-dispersion, evaporation and settling combined, and settling / advection / dispersion / evaporation combined.

Chapter V summarizes our findings with our research and presents recommendations for further research.

Appendix A lists the detailed fuel components for JP-4 and JP-8, formulated by Clewell (4).

Appendix B presents our evaporation / settling model, based on the research of Clewell (4).

II. Literature Review

2.1 Overview

The question we want to answer is: *where and at what magnitude will the air and ground concentrations be as a result of cold startups of aircraft using JP-4 or JP-8 fuel?* Moreover, does the B-52 pose an especially high threat due to its older engine design and higher amount of fuel it deposits into the atmosphere. This process can be quantified by looking at the particle size distribution of the aerosol and determining how long the aerosol stays airborne (the larger particles will settle out due to gravity more quickly, while the smaller particles will remain airborne longer). Next, we must observe how the aerosol advects and disperses. Dispersion determines the concentration of the aerosol at a point, and advection determines the point in space the aerosol has reached. Various sink mechanisms will determine how and to what degree the aerosol settles to the ground. Finally, evaporation will determine the remaining mass and constituent make-up of the JP-4 or JP-8 aerosol over time.

2.2 Lowell, 1959

Lowell, in 1959, studied the effects of jettisoned JP-4 fuel at altitude in a quiet atmosphere. The significant findings of this study as they pertain to this application were in the area of fuel evaporation. Lowell found that temperature was the principle controlling variable for evaporation as initial evaporation rates increased by factors of 15 or more as sea-level temperatures ranged from -30°C to 30°C (17:2). This is more clearly shown by considering initially large (2000 μm) droplets at the temperature extremes. At 30°C, droplets of JP-4 will have lost between 60 and 80 percent of original mass by the

time they reach ground (when jettisoned at altitudes between 3000 and 7000 feet. Conversely, at -30°C , these losses become insignificant (only several percent). Calculating the rate of evaporation requires a knowledge of the ambient conditions, speed of fall of the droplet, temperature of the droplet, size of the droplet at a specific time, and the properties of the fuel (17:12).

2.3 Fuchs, 1964

The classic work on aerosol physics was by N.A. Fuchs in 1964. Fuchs found that the majority of naturally and artificially produced aerosols are very polydisperse (10:5). Hence, the particle size distribution is very important in specifying an aerodisperse system, expressed as either a function of radius or mass of particles. Since it was found that the particle sizes in an aerosol will cover several orders of magnitude, it is customary to use a logarithmic scale to prevent the crowding together of very fine particles (10:9). The distribution of a particular aerosol is very important in classifying the physical characteristics and sink mechanisms of the different groups of particle diameters.

Fuchs found that for aerosols, three forces act on the particles - external forces (gravitational, electrical, etc.), resistance of the medium, and interaction of the particles (the third force being often times neglected because it's in most cases considerably less than the first two forces) (10:21). Fuchs further described the application of Stokes' formula to the settling of aerosol particles under influence of gravity. Stokes' formula shows that the settling velocity of a aerosol is proportional to the square of its diameter and to its density (10:23); so as we increase the particle size in our distribution, settling velocity under gravitational forces increase dramatically.

2.4 Friedlander, 1977

Expanding on the work of Fuchs, S.K. Friedlander emphasized the chemical engineering aspects of aerosols. Aerosols, as Friedlander pointed out, are unstable with respect to coagulation because the reduction in surface area that accompanies particle attachment corresponds to a reduction in the Gibbs free energy under conditions of constant temperature and pressure (9:175). Coagulation is determined from the collisions and resulting attachments of the individual particles in an aerosol. These collision mechanisms include Brownian (thermal) motion and fluid shear under the influence of interacting particle force fields. Because this process is basically nonlinear, it leads to formidable mathematical difficulties.

Particles smaller than $1\text{ }\mu\text{m}$ collide as a result of their Brownian motion, and most of the experimental studies of coagulation are concerned with this mechanism (9:177). Moreover, for particles much larger than the mean free path of the gas (the mean distance traveled by a molecule between successive collisions), experimental evidence suggests that the collision process is limited by diffusion. For particles much smaller than the mean free path of the gas (less than $.1\text{ }\mu\text{m}$), the collision frequency is obtained from the expression derived in the kinetic theory of gases for collision among molecules behaving as rigid elastic spheres (9:179).

This collision frequency becomes modified when particles exert forces on one another (9:182). Van der Waals forces, which are always present, and Coulomb forces (when particles are charged) both contribute such interactive forces. The van der Waals forces, or attractive forces, between uncharged nonpolar molecules is the result of dipoles

produced by fluctuations in the electron clouds, and they tend to increase the collision rate and therefore the coagulation rate of particles (9:184). In the case of electrically charged particles, the particle interaction may be described via induction forces, in addition to the Coulomb force (although induction forces are often neglected because they are relatively small) (9:186). The result of Coulomb forces for such charged particles is again to increase the collision rate (compared to uncharged particles). These interactive forces are important when we consider the general coagulation and condensation equations.

2.5 Clewell, 1983

Building upon the foundation of Lowell, Clewell compared the evaporation of JP-8 to JP-4. Considering that the Air Force had been investigating the environmental effects of jettisoned fuel for years, the concern for Clewell was with the less volatile JP-8. Previously, the fuel jettisoned by the Air Force aircraft was generally JP-4, a highly volatile fuel which is readily dispersed and evaporated, minimizing ground contamination (5:382).

Clewell, using a 270 μm JP-4 droplet, simulated a 1500 meter release height, with three different ground-level temperatures: -20°C , 0°C , 20°C (with the adiabatic lapse rate used to determine temperatures at the 1500 meter release height). In the first few minutes (approximately 5 minutes), Clewell found that the droplet loses from 60 to 90 percent of its mass, depending on the temperature (4:6). Evaporation was therefore found to dominate initially; however, it becomes less important as the droplet eventually reaches the point where it falls without a substantial change in mass (4:8). Component analysis

revealed that the more volatile components in the fuel evaporate preferentially; the lighter components (containing less than eight carbon atoms) are lost almost immediately, while the heavier components (containing more than twelve carbons) experience minimal evaporation (4:12).

As the previous jettisoning studies regarding JP-4 showed (most notably by Lowell), the effect of jettisoning JP-4 at 1500 meters made the final ground fall of JP-4 negligible due to evaporation. Clewell, however, found that the likelihood of significant quantities of the less volatile JP-8 reaching the ground (jettisoned at the same altitude) is much higher and therefore a much more significant environmental concern (5:383).

2.6 Finlayson-Pitts & Pitts, 1986

Finlayson-Pitts and Pitts focused on atmospheric chemistry with regard to aerosols in the atmosphere, as well as expanding on previous aerosol work. Aerosols in the atmosphere range between .002 and 100 μm were of particular interest. The lower end is the smallest size detectable by condensation nuclei counters; the upper end corresponds to the size of fine drizzle and do not remain suspended for a very long period (8:727). The effective diameter of the aerosol particle (which assumes the particle is spherical) depends on the physical properties of the particle, namely its density and surface tension (8:728).

The fine particle category (particles with diameters less than 2.5 μm) is separated into two sub-categories: particles between .08 and 1-2 μm , known as the accumulation range, and particles less than .08 μm , known as the Aitken nuclei range. In practice, no more than two modes of particle ranges are usually seen in any one type of size distribution

(8:737). The coarse particle range is usually produced by mechanical means; hence, if we see a distribution of an aerosol made via a mechanical process, the mass particle distribution will most likely range from the end of the accumulation range to the mechanically-generated (coarse) range (approximately 1 μm to 100 μm) (8:737).

Particles in the accumulation range are typically created from condensation of low volatility vapors and from coagulation of smaller particles in the nuclei range either with themselves or with the larger particles in the accumulation range (8:738). These accumulation range particles may represent a significant portion (e.g. 50%) of the aerosol mass. Because of their smaller particle sizes (versus coarse particles), they have much longer airborne lifetimes (due to much smaller settling velocities from Stokes' law), and are therefore of great interest in atmospheric chemistry.

Applying Stokes' law, it is clear that particles greater than 10 μm have settling velocities greater than .1 cm/s for water and .08 cm/s for JP-8, which settle out of the aerosol relatively quickly (8:756). Particles less than about 1 μm will remain suspended for a long period of time (Stokes' law applies over a considerable range of particle sizes greater than .1 μm) (8:757).

These small particles, although not settling via gravity at a significant rate, do undergo Brownian diffusion. In the absence of convection, particles less than .1 μm are transported primarily by Brownian diffusion due to the rapid coagulation of particles in the Aitken nuclei range (8:756). The rates of Brownian diffusion depends on the concentration gradient; particles tend to diffuse from regions of higher to lower concentrations (8:758).

2.7 Seinfeld, 1986

Seinfeld studied the phenomena of coagulation and condensational growth of aerosols in the 1970's to build upon the previous work by Fuchs and Friedlander. With regard to condensation, he found that the exact solution of the general dynamic equation for aerosol growth by condensation is obtained for particle growth occurring by gas phase diffusion-controlled growth, surface reaction-controlled growth, and volume reaction-controlled growth (in dimensionless form) (24:173). To find the rate of coagulation, it is first necessary to calculate the rate at which particles collide as a result of their Brownian motion; therefore, the Brownian diffusion coefficient (D) for the particles in question is a necessary parameter. The theory is developed by treating one of the particles stationary at the center of the coordinate system and assuming every collision of moving particles with the fixed particle will result in absorption (or coagulation) (24:392). Eventually, after an initially rapid diffusion rate, the rate of coagulation to its steady state value which is proportional to D , R , and N (24:392). The more complex forms of the coagulation equation then build upon this premise. Coagulation may then also be affected by laminar shear flow, turbulence, and by gravitational settling (24:399), as well as by particle force fields (24:401). When coagulation can be neglected, and the only dynamic process influencing individual particles is growth, the size distribution function is governed solely by the condensation equation (24:416). Condensational growth is affected by the growth of each particle and by the source of new particles introduced to the system.

Seinfeld's 1986 work, however, was not limited to aerosols. The work was an all-encompassing study of air pollution and air transport concerns; with regard to air

transport, the stability of the atmosphere is an important consideration. The horizontal eddy diffusion coefficient (K) relates to the stability parameter; essentially, the eddy diffusion coefficient is proportional to the square of the stability parameter (24:597). The stability parameter is affected by the stability of the atmosphere (24:595); therefore, when analyzing the advection and dispersion of an aerosol, parameters such as wind speed and atmospheric stability will play a vital role in quantifying downwind concentration. To predict downwind concentrations, it is necessary to use an appropriate prediction method.

Because of the random motion of the atmosphere, prediction of atmospheric concentrations at various points over all ranges of conditions is a difficult task. Seinfeld mentions two approaches for the prediction of atmospheric concentrations, the Eulerian and Lagrangian approaches. The Eulerian method is based on a material balance over an infinitesimal region fixed in space, whereas the Lagrangian approach is based on considering the particle as it moves through space in the flow (24:552). The deciding factor, however, in judging the validity of either theory for atmospheric diffusion is the comparison of its predictions with experimental data.

Considering the Eulerian theory in a numerical methods approach, the concept of stability plays a key role in the evaluation (24:608). When a method is stable, approximation errors in the solution are suppressed with time. More specifically, with an explicit technique, a restraint is placed on the time step that is used relative to the spatial grid to minimize error and maintain stability. This restriction is that the time change is less than $1/2$ the square of the space step divided by the eddy diffusion coefficient (K) (24:608).

2.8 *Summary*

The reviewed literature points to significant previous research in the area of aerosol science. With the understanding of the aerosol mass distribution, the settling velocities as a function of particle diameter, and the advection-dispersion of the aerosol, this study will elucidate the potential health problems associated with cold startups by quantifying downwind air and ground concentrations of the JP-8 aerosol.

Previous research on the jettisoning of fuel has included the evaporation of the airborne fuel. While the jettisoning studies include fuel droplets with much higher average diameters (rain sized drops), this study is concerned with a much finer size distribution (as well as only looking at the fall of fuel from a height of only a few meters, not from an altitude of hundreds of meters). The effect of the colder temperatures, causing a decrease in the evaporation of the JP-8, may prove significant in the quantification of air and ground concentrations.

III. Methodology

3.1 Overview

We present the solution to our research question by identifying and justifying the key assumptions that go into our model. To establish the structural framework of our model, it is first important to establish the theoretical aerosol mass distribution for our plume; moreover, we make use of Stokes' formula to establish how the aerosol mass settles out of the moving airborne plume. Then, we must describe the structural framework of our model by describing how we are modeling the critical chemical and physical processes: evaporation, advection, and dispersion.

To describe the aerosol concentration in the air for the purpose of inhalation and skin exposure studies, as well as the aerosol concentration which reaches the ground, we need to know the following:

1. What is the amount emitted?
2. What are the dispersion rates imposed by the atmosphere?
3. What are the magnitudes of evaporation and settling which are taking place?

3.2 Initial Conditions

3.2.1 Plume Composition. We assume a distribution based on the findings by Pitts (8). The plume will have a mass distribution for diameters ranging from 1 to 100 μm , which represents the mechanically-generated aerosol range (8:737). The mechanically generated range will also represent the entire portion of the aerosol mass, as it is necessary to convert the size distribution of our aerosol to a mass distribution. The mass distribution has the same appearance as the size distribution, just shifted to the right (8:749). The

findings by Pitts, combined with the empirical evidence of what is happening in the field, justify the assumption of using a 1 to 100 μm aerosol size distribution.

3.2.2 Plume Geometry. We assume that the plume is a continuous point source for 10 minutes, then it becomes an instantaneous point source as it is emitted into the atmosphere from the aircraft. The cold start-up process takes approximately 10 minutes, so we assume a volume, mass, and concentration of the plume after the entire plume accumulates after this cold start-up process; at time zero, the entire plume mass as result of the uncombusted emission of the fuel is airborne and only affected by gravity and wind for movement. The source term (in mass of aerosol emitted from the aircraft with time) is employed here.

3.2.3 Plume Diameter Distribution. We employ the log-normal distribution to describe the distribution of our aerosol mass (10:12):

$$P(x, \mu, \sigma) = \log n(x, \mu, \sigma) = \frac{1}{\sqrt{2\pi}\sigma} \exp\left[-\frac{(\ln(x) - \mu)^2}{2\sigma^2}\right] \quad (3.1)$$

where P is the probability that the diameter of the aerosol in the distribution is equal to x , μ is the average diameter in the distribution, and σ is the standard deviation. We choose 3 μm as the average diameter, and this is a reasonable assumption (8:737). We then choose a standard deviation (approximately 0.8) that causes the distribution to encompass the range of interest in this study (1 to 100 μm).

Since we are interested in the mass distribution of the particles of the aerosol as we are tracking aerosol mass downwind, we use the Hatch-Choate method (8:751) of converting a number distribution to a mass distribution:

$$\frac{D_{gM}}{D_{gN}} = \exp(b \ln^2 \sigma) \quad (3.2)$$

where b for the conversion of number to mass distribution is 3.0, D_{gM} is the mean diameter of the mass distribution, σ is the standard deviation for both number and mass distributions (8:749), and D_{gN} is the mean diameter of the number distribution.

Fuchs found that the log-normal distribution is appropriate to physically describe the distribution of aerosols (10:9). To answer the question of why we employ the log-normal distribution, we must describe the type of distribution we need for our purposes. We need a function that is defined only for diameters greater than zero and approaches zero as the diameter approaches infinity (24:281). The log-normal distribution satisfies this criteria. Moreover, a distribution that is log-normally distributed has its logarithm governed by a normal distribution, making it a popular one for representing aerosol size distributions (24:282).

3.3 Plume Settling

3.3.1 Method of Settling. We assume that most of the aerosol mass will settle via gravity relatively quickly due to the relatively large size of the droplet diameters. At the high end of the mass distribution, the droplets will settle to the ground in approximately 4 seconds; however, the suspension time goes up with the square of the droplet diameter as the droplet gets smaller, as we observe with equation 3.3 in the next section (8:757). Our

grid will represent the width of the plume as well as the distance it takes for the entire aerosol to settle to the ground.

3.3.2 Stokes' Formula. Stokes' law governs the behavior of the aerosol under the influence of gravitational settling:

$$v = \frac{D^2 \rho g}{18\eta} \quad (3.3)$$

where v is the settling velocity, D is the particle diameter, ρ is the particle density, g is the acceleration of gravity (9.8 meters per second squared), and η is the gas viscosity. However, the above equation only applies for diameters greater than 1.5 μm because its derivation is based on the assumption that the relative speed of the air at the surface of the particle is zero (8:754). However, as the particle becomes smaller, the surrounding air particles are less of a continuous fluid and more like discrete molecules separated by space through which the particles can "slip", with the net effect being that the particles can move faster than predicted via equation 3.3 (8:755). Therefore, we must employ the Cunningham correction factor for the particles smaller than 1.5 μm . The resulting correction factor (equation 3.4) must then be multiplied by equation 3.3 for particles under 1.5 μm :

$$C = 1 + \frac{2514L}{D} \quad (3.4)$$

where C is the Cunningham correction factor, D is the particle diameter, and L is the mean free path between air molecule collisions defined as the average distance traveled between collisions with another molecule.

Our calculations will keep track of the aerosol as it settles out of the plume (due to gravity) as it moves downwind. The effects of coagulation will be neglected because we are looking at a range where coagulation is not as significant (coagulation becomes more significant for particles less than .08 μm) (8:738). Moreover, since we are concerned with a mist (liquid particles), condensation will not play as important a role in our model due to the difficulty for condensation to occur with liquid particles as opposed to solid particles. Therefore, it is a reasonable assumption, given our type of aerosol and distribution, to take the initial distribution as a constant and to look only at the effect of gravity with regard to downwind settling.

3.4 Plume Advection and Dispersion

3.4.1 The Atmospheric Diffusion Equation. The atmospheric diffusion equation in the absence of chemical reaction is:

$$\frac{\partial}{\partial t} C + u \frac{\partial}{\partial x} C + v \frac{\partial}{\partial y} C + w \frac{\partial}{\partial z} C = K_{xx} \frac{\partial^2}{\partial x^2} C + K_{yy} \frac{\partial^2}{\partial y^2} C + K_{zz} \frac{\partial^2}{\partial z^2} C \quad (3.5)$$

where C = the concentration of the aerosol; u, v, w are the mean wind speeds in the x, y, z directions; K_{xx} , K_{yy} , and K_{zz} the eddy diffusivity parameters in the x, y, z directions. The atmospheric diffusion equation provides a general approach to atmospheric diffusion calculations, with the ability to include nonlinear chemical reactions and changes in wind speed with height (24:593).

The problem then becomes obtaining appropriate wind speeds, eddy diffusivities, and a method of numerically calculating downwind concentration as a function of time and space. The following sections will address these areas and list pertinent assumptions.

3.4.2 Advection. Advection is the effect of wind on the cloud in question. Since we are modeling the movement of the cloud through space, we are taking into account wind speed in the x,y, and z directions. However, we can assume that wind will be predominantly in one direction, and essentially zero in the other directions; we choose our coordinate system so the wind is in the x-direction. We consider the wind speed to be three different values in the x-direction: 1, 3, and 5 m/s (at the point source, which is at an altitude of 3 meters), and as already stated, assume that the mean wind speed is zero in the y and z directions in our model (thereby simplifying the above equation 3.5). With our assumption of the wind speed at an altitude of 3 meters, we must convert to a mean wind speed at an altitude of 10 meters so that we may use stability parameters that are measured at 10 meters altitude (24:593). The following is the power-law function of height:

$$\frac{u}{u_r} = \left(\frac{z}{z_r} \right)^p \quad (3.6)$$

where p depends on the stability of the atmosphere.

3.4.3 Dispersion. Dispersion is the effect of the aerosol mass becoming diluted with the surrounding atmosphere as it moves through space and time. The eddy diffusivities will be the parameters for this behavior, as equation (3.5) suggests. An important assumption in the equation is that molecular diffusion is negligible and the primary mechanism affecting concentration is atmospheric turbulence, parameterized by K in all directions (24:522).

We will assume that atmospheric stability will be the same in the x,y,z directions, or that $K_{xx}=K_{yy}=K_{zz}$. We will look at three different values of eddy diffusivities, representing the range of stability classes from A-D. Since we are interested in the airborne concentration (micrograms per cubic meter) as the plume moves downwind, we will relate the effect of the different ranges of eddy diffusivities on the concentration. The eddy diffusivity is related to the stability parameter via the following (for the cross-wind case):

$$K_{yy} = \frac{1}{2} \frac{d\sigma_y^2}{dt} \quad (3.7)$$

where σ is the stability parameter (24:597). Of course σ will vary depending on the stability class (A-F) of the atmosphere, ranging from unstable to stable.

3.4.4 Gaussian Solution to Atmospheric Diffusion Equation. The Gaussian solution to the general atmospheric diffusion equation 3.5 is then (24:570):

$$C(x, y, z) = \frac{q}{2\pi u \sigma_y \sigma_z} \exp\left(\frac{-y^2}{2\sigma_y^2}\right) \left[\exp\left[\frac{-(z-H)^2}{2\sigma_z^2}\right] + \exp\left[\frac{-(z+H)^2}{2\sigma_z^2}\right] \right] \quad (3.8)$$

$$C(x, y, z, t) = \frac{S}{(2\pi)^{\frac{3}{2}} (\sigma_x \sigma_y \sigma_z)^{\frac{1}{2}}} \exp\left[-\frac{(x-ut)^2}{2\sigma_x^2} - \frac{y^2}{2\sigma_y^2} - \frac{z^2}{2\sigma_z^2}\right] \quad (3.9)$$

where equation (3.8) is for the continuous point source and (3.9) is for the instantaneous point source; q (in eqn. 3.8) is a mass flowrate term, while S (in eqn. 3.9) is a mass term.

To determine the dispersion parameters (σ_x , σ_y , σ_z) in equations 3.8 and 3.9, it is necessary to use the Pasquill-Gifford coefficients for R_y where $R_y = .384$, $.27$, and $.179$, respectively, for stability classes A-B, B-C, and C-D (24:577). The dispersion parameters are computed via the following:

$$\sigma_y(x) = R_y x^{.894} \quad (3.10)$$

where x is the distance from the source; this model assumes $\sigma_x = \sigma_y = \sigma_z$.

3.5 Evaporation

3.5.1 Assumptions. We use the work previously developed by Lowell and Clewell for the evaporation calculations in our model. The following physical assumptions apply to our evaporation model.

1. *Molecular effects are negligible.* Lowell concluded that this assumption slightly overestimates the evaporation of fuel droplets in the plume. However, Lowell concluded that this would have a small affect in the solution and that the assumption is reasonable (17:3). Once the mass has evaporated from the droplet, we no longer include it to be part of our model.
2. *Droplets fall independently.* We do not consider the entrainment of smaller drops by the larger drops falling faster due to Stokes' formula.
3. *The evaporation of a fuel droplet can be calculated by a mixture of known components.* By this assumption we also assume that there is a uniform distribution of components in the droplet.

3.5.2 *Evaporation Formula.* Mass loss of the droplet is computed via the Lowell model (17:3), using the following step-wise approximation.

$$\frac{1}{\pi D^2} \frac{d}{dt} M_i = h_{m,i} p_i \epsilon_i \quad (3.11)$$

where M_i = mass of i'th component of droplet

D = droplet diameter

$h_{m,i}$ = mass transfer coefficient of the i'th component

p_i = vapor pressure of the i'th component

ϵ_i = mole fraction of the i'th component

This approximation (after integration) then becomes:

$$\Delta M_i = \pi D^2 h_{m,i} p_i \epsilon_i \Delta t \quad (3.12)$$

We assume that our Δt is small enough so that D , h , p , and ϵ are approximately constant (4:88). This formula shows that the loss in mass with time of a droplet is directly proportional to the square of the diameter of the droplet. The total mass loss therefore becomes more significant at the higher end of our droplet distribution; however, the percentage of mass loss will decrease with increasing diameter because the volume (which is being divided) is in terms of the radius cubed. Moreover, the more volatile components will evaporate relatively quickly for a given droplet in our model.

According to Clewell, we must calculate a new droplet mass from the previous droplet mass in order to calculate a new density for each component (4:87). We may then calculate the new droplet volume by summing over the n components of the fuel mixture:

$$V = \sum_{i=1}^n V_i = \sum_{i=1}^n \frac{m_i}{\rho_i} \quad (3.13)$$

where ρ_i is the new density of the i 'th component and m_i is the new mass of the i 'th component. Assuming that the droplet is a perfect sphere, we arrive at an expression for the ever-changing radius, R :

$$R = \left(\frac{3}{4\pi} \sum_{i=1}^n \frac{m_i}{\rho_i} \right)^{\frac{1}{3}} \quad (3.14)$$

With the change in mass, we may compute a heat balance as well as the change in droplet temperature. We bring the droplet into thermodynamic equilibrium by imposing Clewell's requirement: the mass loss in any interval will be no more than what our step-wise calculation of heat-loss is able to bring into a steady-state temperature with the local air temperature (4:95). With this requirement, we ensure thermodynamic equilibrium of the droplet, thus ensuring that the mass loss of the droplet with time is not unreasonable.

3.5.3 Design Considerations. For our model, evaporation will be simulated by using a small time step and keeping track of the mass loss for each component of each diameter size.

As noted by Lowell and Clewell, temperature is the most influential physical parameter (by affecting vapor pressure) in calculating evaporation. We will employ 3 different temperatures (-20, 0, and 20 degrees Celsius) to witness the effect that temperature has on our solution.

3.6 Numerical Methods

3.6.1 Lagrangian Assumption. We are using a classical Lagrangian approach with our origin advecting with the direction of the wind. Moreover, we employ the assumption that the behavior of the plume will be described relative to a fixed coordinate system (24:526).

3.6.2 Solution of the Diffusion Equation. Because we are assuming that the plume is a aerosol mass formed after a certain period of time for cold start-up (10 minutes), we assume that the plume is an instantaneous source after this time (and a continuous source during the cold start-up process). In using a numerical method, we assume that the time step involved is small enough so that we may use a numerical approximation from one point in time to the next using this sufficiently small, discrete time step. From the diffusion equation (3.5), we obtain the finite difference approximation:

$$C_{n+1,i} = C_n + \frac{K_{xx}\Delta t}{\Delta x^2} (C_{n,i+1} - 2C_{n,i} + C_{n,i-1}) - u \left[\frac{\Delta t (C_{n,i+1} - C_{n,i-1})}{2\Delta x} \right] \quad (3.15)$$

where n (in the concentration expression, C) represents time and i represents grid size for the plume; Δt represents the time step; Δx represents the step through space (as plume moves downwind).

However, there exists a stability requirement that limits the time step relative to the space step in order to keep the error in our approximation (equation 3.15) to a manageable level. The following is the stability requirement:

$$\frac{K_{xx}\Delta t}{\Delta x^2} \leq \frac{1}{2} \quad (3.16)$$

3.6.3 The 3-D Case. Equations 3.15 and 3.16 give us our numerical approximation for a one-dimensional case (in the x-direction). We must represent the 3-D plume as it advects and disperses downwind. For employment of the 3-D numerical solution, we take an assumption proposed by Seinfeld for a simple case and further developed by Pffeifer (20:3-21). This assumption states that the 3-D numerical solution to equation 3.5 is separable (24:535) and subject to the following conditions:

$$C(x, y, z) = S\delta(x)\delta(y)\delta(z) \quad (3.17)$$

$$C(x, y, z, t) = 0 \quad (\text{as } x, y, z \text{ goes to } \pm \infty) \quad (3.18)$$

where S is the source term of the plume.

For this 3-D case, equation 3.16 would be modified by dividing the right side of the equation by 3 for the following result:

$$\frac{K_{xx}\Delta t}{\Delta x^2} \leq \frac{1}{6} \quad (3.19)$$

The same condition above would apply for the y and z directions.

Equation 3.15 would also be modified to reflect the 3-D nature of our plume. Because of our assumption of separation of variables, we may therefore solve for y and z exactly as we did for x in equation 3.15 and multiply the three results together for the final form of our numerical approximation.

3.7 Summary

Now that we have developed the methodology for solving the problem at hand, we proceed with the running of our model. What we will ultimately witness is the movement

(advection) of this aerosol plume downwind, the deposition of aerosol mass as it moves downwind, the evaporation of airborne and ground fall fuel mass with time, and the dispersion of aerosol mass with time. This model will therefore give us the air and ground concentrations of the aerosol as we move downwind, thereby exposing possible health risks due to inhalation and/or seepage into groundwater.

IV. Model Results

4.1 Overview

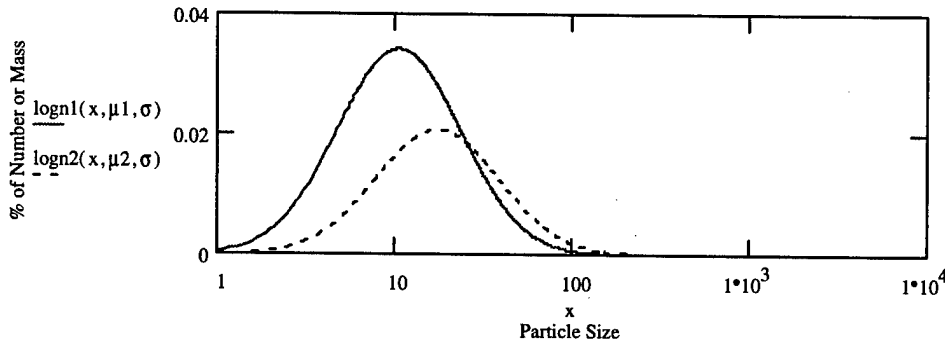
In this chapter we present results generated from our model, keeping in mind the pertinent questions that we must address: how the aerosol settles, how the aerosol advects and disperses downwind, how it evaporates, and are the concentrations high enough such that there are health concerns? We begin answering these questions by investigating the aerosol settling as a function of its mass distribution. Then we observe the advection and dispersion of the airborne aerosol as we solve the Gaussian equations (3.8) and (3.9). The evaporation with time of the aerosol is investigated as we are interested in the mass loss with time of the particular droplets, as well as the mass loss of the individual components of the JP-8 droplet with time. Finally, we investigate the combined effects of the above phenomena, as well as the health implications.

4.2 Aerosol Settling.

4.2.1 Count Versus Mass Distribution. We began our model by assuming a distribution of particle sizes from our mechanically generated aerosol range. From Finlayson-Pitts (8:737), the distribution based on number will range from approximately 1 to 100 μm (in the mechanically generated range). We convert this to a mass distribution using equation (3.2) and the mean and standard deviation of the number distribution. In our application, we began with a number distribution with a mean and standard deviation of 3.0 and 0.8, respectively, giving us a distribution range from 1 to 100 μm . This corresponds to a mass distribution with mean and standard deviation of 3.5 and 0.8, respectively, giving a distribution range from approximately 5 to 300 μm . The

plot of the count (or number) distribution versus the mass distribution (log scale on the x-axis) of our aerosol is then:

Figure 4.1: Comparison of Count Distribution Versus Mass Distribution of Particles



As the graph shows, we skew the distribution to the right as expected when we go from the number distribution to the mass distribution. Since we are above $1.5 \mu\text{m}$ in the mass distribution range, we do not need the correction factor in calculating the Stokes' velocity.

4.2.2 Time to Ground of the Aerosol. In assessing the time to ground of our aerosol mass, we employ the Stokes' relationship to our range of particle sizes. As a first look at the settling, we ignore evaporation. Later, in section 4.4, we consider both evaporation and settling. Since we are observing a range of sizes between 5 and $300 \mu\text{m}$, we split up the entire range into 18 separate diameter ranges. We take the average diameter in the range to calculate the velocity in cm/s and time in seconds to reach the ground (3 m). The mass per diameter range is calculated by making use of the cumulative distribution

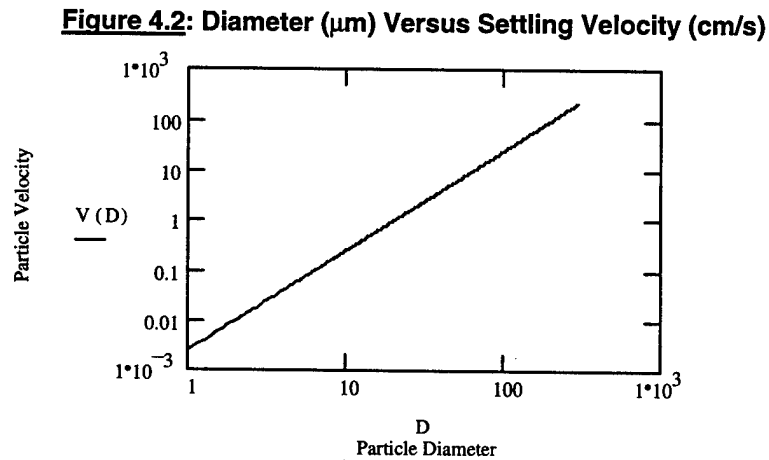
function of the lognormal distribution for our mass. The following table summarizes the range of our particle sizes (for the mass distribution):

Table 4.1: Comparison of Diameter, Mass, Settling Velocities (cm/s) and Time (s).

Diameter Range	Average Diam.	Percent Mass	Vel of Avg Diam	Time to Ground
5-10	7.5	6.7	0.14	2222
10-20	15	19.7	0.54	556
20-30	25	18.7	1.50	200
30-40	35	14.2	2.94	102
40-50	45	10.3	4.86	61.7
50-60	55	7.5	7.26	41.3
60-70	65	5.4	10.14	29.6
70-80	75	4.0	13.50	22.2
80-90	85	2.9	17.34	17.3
90-100	95	2.2	21.66	13.9
100-110	105	1.7	26.46	11.3
110-120	115	1.3	31.74	9.5
120-130	125	1.0	37.50	8.0
130-140	135	0.8	43.74	6.9
140-150	145	0.6	50.46	6.0
150-200	175	1.7	73.50	4.1
200-250	225	0.7	121.50	2.5
250-300	275	0.3	181.50	1.7

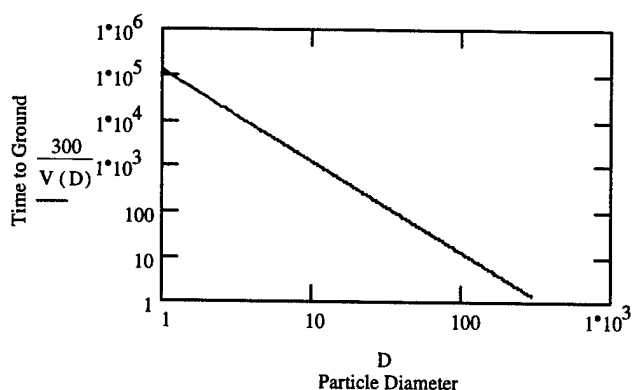
We see from the results of Table 4.1 that our fuel mass will settle to the ground within approximately 2200 seconds, or about 37 minutes; moreover, 93% of the mass will settle to the ground in under 10 minutes (556 seconds). For droplet diameters under 10 μm , the

time to ground starts to increase dramatically. Droplets in the 1 to 5 μm range are neglected because they contribute negligible mass in our mass distribution. The relationship between the particle size and its corresponding settling velocity is plotted in Figure 4.2 using a log-log scale:



Because the velocity data in Table 4.1 were calculated using equation (3.3), Figure 4.2 can be thought of as a plot of equation (3.3), which is Stokes' Law. To convert from velocity to time in seconds for the particle to fall from the aircraft emission source to the ground (approximately 3 meters), we simply take the reciprocal of the velocity and multiply by 300 cm. The following graph shows this relationship of diameter versus time to ground, and as we would expect, the curve is exactly opposite of the previous relationship:

Figure 4.3: Diameter (μm) Versus Time (s) To Reach Ground



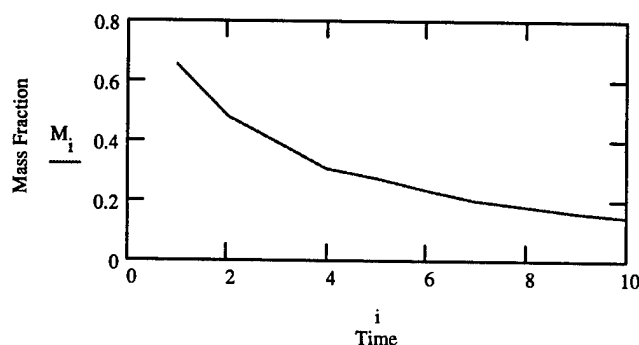
Next, we wish to observe what percentage of mass of fuel remains airborne as a function of time. After 1 minute, only droplets with diameters larger than 50 μm remain airborne, so 65% of the mass is left. These percentages were calculated for each subsequent minute, resulting in the data of Table 4.2:

Table 4.2: Values of Time (min) vs. Mass Remaining (%) of the Airborne Aerosol

Time	1min	2min	3min	4min	5min	6min	7min	8min	9min	10min
Mass	65%	48%	39%	31%	27%	23%	20%	18%	16%	15%

The following graph depicts this relationship:

Figure 4.4: Time (min) vs. Mass Remaining (%)



As expected, we observe a marked decrease in mass the first few minutes of the warm-up process; however, this decrease in mass begins to slow down as we see the increasing time it takes the smaller particle sizes to settle to the ground via Stokes' formula.

4.3 Aerosol Advection and Dispersion.

4.3.1 Assumption of Point Source. We assume that our cloud will be generated via a continuous point source for the first ten minutes of our simulation, representing the cold-startup procedure. After this initial start-up procedure, we assume that the cloud is an instantaneous point source.

4.3.2 Atmospheric Variation. We assume 3 different cases for wind speed at our source 3 meters above the ground: 1, 3, and 5 m/s. From Seinfeld (24:593), these wind speeds at 3 meters are converted to wind speed at 10 meters above ground, the standard height for which wind speed is measured. Using equation (3.6) and using different values of the p variable for our different stability classes, we find that our 3 cases translate to approximately 1.2, 3.6, and 6.5 m/s at 10 meters, which gives us stability classes A-B, B-C, and C-D. We see that by assuming different wind speeds, the plume/cloud advects in varying degrees. These wind speeds give us different atmospheric stability classes (24:509), which also affect dispersion of our plume/cloud. Stability classes E and F are disregarded because we assume daylight operations with variable amounts of incoming solar radiation. Since our three stability classes all include ranges, we take the average value in that range to use for our Gaussian plume parameter coefficients (24:577).

4.3.3 Continuous Source. For the continuous point source, we consider a B-52H at idle, emitting uncombusted fuel aerosol for an assumed 10 minutes during this cold startup process. The engine of the B-52H is the TF33-3, which emits 0.21 lbs/hr, equating to approximately 211,867 micrograms per second. Since the fuel aerosol coming out of the engine during this cold startup process is influenced by turbulent motion, we assume that the plume will be influenced solely by atmospheric conditions soon after being emitted. At this point, we look at the three cases for stability of the atmosphere, influenced by the three different cases for wind speed. Another assumption in our downwind concentration analysis is that we are observing the maximum downwind concentration with distance. Hence, we first look at the maximum concentration of the plume as it moves downwind ($y=0$ and $x=u*t$); secondly, we look at the dispersion of the plume in the y -direction as it moves downwind. In all cases, we take $h=0$ and $z=0$ because the B-52 emission is essentially at ground level. Figure 4.5 shows the maximum downwind concentration as a function of distance for the first case (A-B), and Table 4.3 shows the dispersion of the concentration in the $\pm y$ direction (± 4 meters). These concentrations are calculated using equations (3.8) and (3.10) with $q=211,867 \mu\text{g/s}$, $R_y=.384$, and $u = 1\text{m/s}$ (while $y, z, H = 0$ for maximum conditions).

Figure 4.5: Dist. (m) vs. Max. Downwind Conc. ($\mu\text{g}/\text{m}^3$), Cont Source (case A-B)

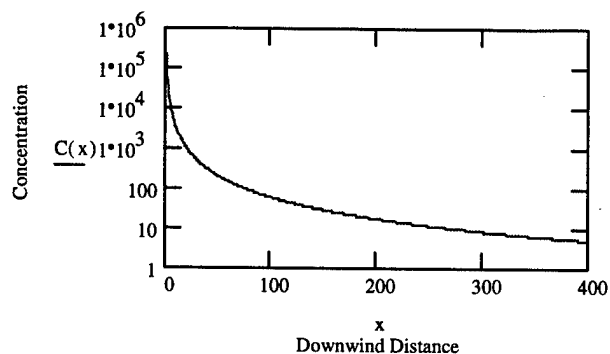


Table 4.3: Concentration ($\mu\text{g}/\text{m}^3$) in the +/- Y Direction (m), Cont Source (case A-B).

Dist	y=-4	y=-3	y=-2	y=-1	y=0	y=1	y=2	y=3	y=4
1m	0	1.28E-8	0.294	7.70E3	2.29E5	7.70E3	0.294	1.28E-8	0
5m	608	2.31E3	6.0E3	1.06E4	1.29E4	1.06E4	6.0E3	2.31E3	608
10m	1.54E3	2.27E3	2.99E3	3.53E3	3.73E3	3.53E3	2.99E3	2.27E3	1.54E3
20m	835	934	1.01E3	1.06E3	1.08E3	1.06E3	1.01E3	934	835
50m	199	204	207	209	210	209	207	204	199
59m	150	153	154	156	156	156	154	153	150
75m	99	100	101	101	102	101	101	100	99
100m	60	60	60	61	61	61	60	60	60

As we see from the above table, the concentration starts out at the center and quickly disperses in the y-direction until (at approximately 75m) the concentration is virtually constant for $-4 \text{ meters} < y < 4 \text{ meters}$. The concentration at the 59m mark shows where the concentration goes below the hydrocarbon standard of $160 \mu\text{g}/\text{m}^3$ as given by USEPA (29:51). The stability parameters change with distance from the source, and the stability parameters were taken from Seinfeld by averaging the A and B coefficients for R_y (24:577). It was noted above that we are assuming atmospheric and not turbulent conditions dictate the motion of our plume; moreover, since Stokes' Law applies to

laminar and not turbulent flow, we assume that the aerosol mass will transition from turbulent to laminar flow when atmospheric conditions take over at that point.

For the B-C case, we see a decrease in the concentration even though the increased stability of the atmosphere would suggest that concentration downwind would rise due to less dispersion in the y and z direction. This is due to the increased wind velocity, which helps to disperse the plume in the x-direction. Figure 4.6 and Table 4.4 show the B-C case for maximum downwind concentration and dispersion in the y-direction. These concentrations are calculated using equations (3.8) and (3.10) with $q=211,867 \mu\text{g/s}$, $R_y=.270$, and $u = 3\text{m/s}$ (while $y, z, H = 0$ for maximum conditions).

Figure 4.6: Dist. (m) vs. Max. Downwind Conc. ($\mu\text{g/m}^3$), Cont Source (case B-C)

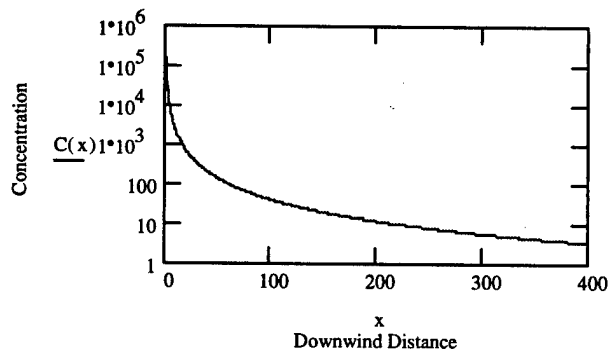


Table 4.4: Concentration ($\mu\text{g}/\text{m}^3$) in the +/- Y Direction (m), Cont Source (case B-C).

Dist	Y=-4	Y=-3	Y=-2	Y=-1	Y=0	Y=1	Y=2	Y=3	Y=4
1m	0	0	1.88E-7	167	1.54E5	167	1.88E-7	0	0
5m	18.1	269	1.85E3	5.90E3	8.68E3	5.90E3	1.85E3	269	18.1
10m	420	919	1.61E3	2.25E3	2.51E3	2.25E3	1.61E3	919	420
20m	433	544	639	704	727	704	639	544	433
47m	141	148	154	157	158	157	154	148	141
50m	128	134	138	140	141	140	138	134	128
75m	65	67	68	68	68	68	68	67	65
100m	40	40	41	41	41	41	41	40	40

As we observe for the B-C case, the concentration goes below the hydrocarbon standard at the 47 meter mark.

For the C-D case, the increased stability (which decreases dispersion) overcompensates for the increase in wind velocity which increases stability, as we see from the following. These concentrations are calculated using equations (3.8) and (3.10) with $q=211,867 \mu\text{g}/\text{s}$, $R_y=.179$, and $u = 5\text{m}/\text{s}$ (while $y, z, H = 0$ for maximum conditions).

Figure 4.7: Dist. (m) vs. Max. Downwind Conc. ($\mu\text{g}/\text{m}^3$), Cont Source (case C-D)

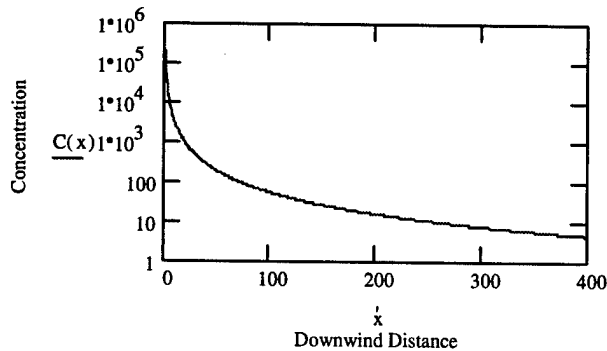


Table 4.5: Concentration ($\mu\text{g}/\text{m}^3$) in the +/- Y Direction (m), Cont Source (case C-D).

Dist	Y=-4	Y=-3	Y=-2	Y=-1	Y=0	Y=1	Y=2	Y=3	Y=4
1m	0	0	0	0.035	2.11E5	0.035	0	0	0
5m	9.38E-3	4.38	353	4.92E3	1.18E4	4.92E3	353	4.38	9.38E-3
10m	58.7	348	1.24E3	2.66E3	3.43E3	2.66E3	1.24E3	348	58.7
20m	306	512	740	923	993	923	740	512	306
50m	153	170	182	190	193	190	182	170	153
56m	131	142	150	156	158	156	150	142	131
75m	84	88	91	93	93	93	91	88	84
100m	52	54	55	56	56	56	55	54	52

As the concentration increased downwind from the B-C case, we see that the maximum concentration downwind goes below the hydrocarbon standard at 56 meters. Next, we observe that when the engine begins to combust the fuel, we must assume that the emitted fuel is essentially an instantaneous cloud and no longer a continuous source.

4.3.4 Instantaneous Source. For an instantaneous source, we assume that the 10 minutes of cold startup created a fuel cloud mass approximately equal to the emission rate times the cold startup time. Of course, we must take into account the deposition of the aerosol mass due to Stokes' Law (see table 4.2); therefore, we compensate for the lost mass by adjusting the total aerosol mass emitted in ten minutes ($1.27 \times 10^8 \mu\text{g}$) to the amount remaining after ten minutes due to deposition ($3.84 \times 10^7 \mu\text{g}$), which accounts for about 30% of the total; hence, 70% of the mass is deposited on the ground during this ten minute interval.

Figure 4.8 and Table 4.6 show the dispersion of our aerosol mass for case A-B if we assume the aerosol mass is 30% of the total emitted after 10 minutes. In Figure 4.8 we see that the maximum cloud mass concentration decreases with time, while in Table 4.6 we see that the cloud mass distributes itself in the y-direction with time until (at 106m downwind) the concentration is evenly distributed from $y=-4$ to $y=4$ meters (as we observed with the continuous case). Since we are only concerned with maximum downwind concentration, we keep track of the time by dividing the distance downwind by the velocity we are assuming, depending on the stability class we assume (1, 3 and 5 m/s, respectively). These concentrations are calculated using equations (3.9) and (3.10) with $S=3.84 \times 10^7 \mu\text{g}$ and $R_y=.384$ (while $u, x, y, z = 0$ for maximum conditions; advection already accounted for).

Figure 4.8: Dist. (m) vs. Max. Downwind Conc. ($\mu\text{g}/\text{m}^3$), Inst Source (case A-B)

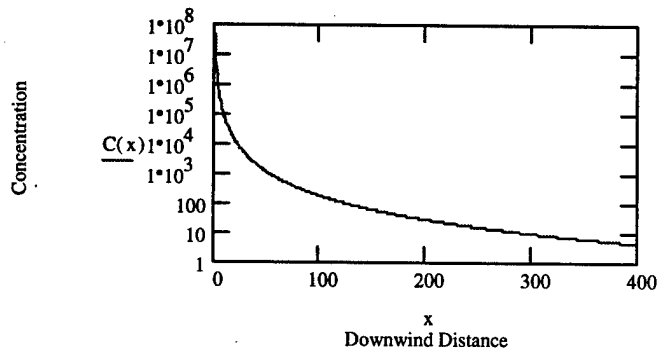


Table 4.6: Concentration ($\mu\text{g}/\text{m}^3$) in the +/- Y Direction (m), Inst Source (case A-B).

Dist	Y=-4	Y=-3	Y=-2	Y=-1	Y=0	Y=1	Y=2	Y=3	Y=4
1m	0	2.40E-6	55.4	1.45E6	4.31E7	1.45E6	55.4	2.40E-6	0
5m	2.72E4	1.03E5	2.68E5	4.74E5	5.75E5	4.74E5	2.68E5	1.03E5	2.72E4
10m	3.70E4	5.45E4	7.18E4	8.47E4	8.96E4	8.47E4	7.18E4	5.45E4	3.70E4
20m	1.08E4	1.21E4	1.31E4	1.37E4	1.40E4	1.37E4	1.31E4	1.21E4	1.08E4
50m	1.14E3	1.16E3	1.18E3	1.19E3	1.20E3	1.19E3	1.18E3	1.16E3	1.14E3
100m	184	185	186	186	186	186	186	185	184
106m	157	158	159	159	159	159	159	158	157
150m	62	63	63	63	63	63	63	63	62

As we see from the previous results, the dispersion in the y-direction takes place much more rapidly then for the continuous case. Since we assume ten minutes emission, this affects how long downwind we have to concerned with airborne concentration; hence, with our source term, we see that the concentration goes below the hydrocarbon standard at the 106 meter mark.

For the cloud, we do not have the dispersion of the concentration affected by the wind speed directly as we did for our plume; rather, the wind speed only affects the concentration in that (once again) the stability classes are changed and dispersion hindered with higher stability. We need to once again concern ourselves with the change in the stability parameters (increase) with distance from source. Hence, for our cloud we only see an increase in downwind concentration with increasing stability, as we see with case B-C (Figure 4.9 and Table 4.7). These concentrations are calculated using equations

(3.9) and (3.10) with $S=3.84 \times 10^7 \mu\text{g}$ and $R_y = .270$ (while $u, x, y, z = 0$ for maximum conditions; advection already accounted for).

Figure 4.9: Dist. (m) vs. Max. Downwind Conc. ($\mu\text{g}/\text{m}^3$), Inst Source (case B-C)

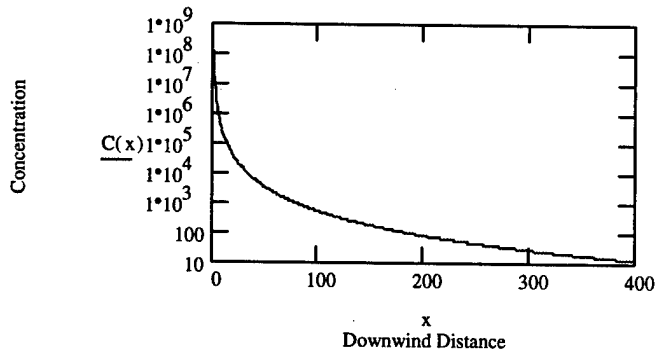


Table 4.7: Concentration ($\mu\text{g}/\text{m}^3$) in the +/- Y Direction (m), Inst Source (case B-C)

Dist	Y=-4	Y=-3	Y=-2	Y=-1	Y=0	Y=1	Y=2	Y=3	Y=4
1m	0	0	1.51E-4	1.30E5	1.24E8	1.30E5	1.51E-4	0	0
5m	3.44E3	5.13E4	3.53E5	1.12E6	1.65E6	1.12E6	3.53E5	5.13E4	3.44E3
10m	4.31E4	9.42E4	1.65E5	2.30E5	2.58E5	2.30E5	1.65E5	9.42E4	4.31E4
20m	2.39E4	3.0E4	3.53E4	3.89E4	4.01E4	3.89E4	3.53E4	3.0E4	2.39E4
50m	3.11E3	3.25E3	3.35E3	3.42E3	3.44E3	3.42E3	3.35E3	3.25E3	3.11E3
100m	520	527	532	535	536	535	532	527	520
157m	158	159	159	160	160	160	159	159	158
200m	83	83	83	83	83	83	83	83	83

With the B-C stability class, we see that the “critical” distance is 157 meters versus 106 meters for the A-B stability class as a result of the increased stability of this stability

class. We already see that increased stability for the case of an instantaneous source affects downwind concentration much more than for the continuous case.

For our C-D case, we see this trend of increasing concentration even more pronounced, as shown in Figure 4.10 and Table 4.8. These concentrations are calculated using equations (3.9) and (3.10) with $S=3.84 \times 10^7 \mu\text{g}$ and $R_y=.179$ (with $u, x, y, z = 0$ for maximum conditions; advection already accounted for).

Figure 4.10: Dist. (m) vs. Max. Downwind Conc. ($\mu\text{g}/\text{m}^3$), Inst Source (case C-D)

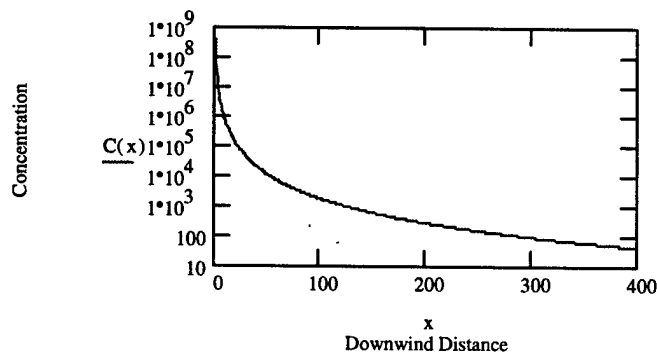


Table 4.8: Concentration ($\mu\text{g}/\text{m}^3$) in the +/- Y Direction (m), Inst Source (case C-D)

Dist	Y=-4	Y=-3	Y=-2	Y=-1	Y=0	Y=1	Y=2	Y=3	Y=4
1m	0	0	0	71	4.25E8	71	0	0	0
5m	4.5	2.10E3	1.69E3	2.36E6	5.67E6	2.36E6	1.69E3	2.10E3	4.5
10m	1.51E4	8.97E4	3.20E5	6.86E5	8.84E5	6.86E5	3.20E5	8.97E4	1.51E4
50m	9.39E3	1.04E4	1.11E4	1.16E4	1.18E4	1.16E4	1.11E4	1.04E4	9.39E3
100m	1.72E3	1.77E3	1.81E3	1.83E3	1.84E3	1.83E3	1.81E3	1.77E3	1.72E3
200m	281	283	285	286	287	286	285	283	281
249m	157	158	159	159	159	159	159	158	157
300m	96	96	96	97	97	97	96	96	96

We see once again the affect of an increased stability class on our results as we observe a new critical distance of 249 meters for the C-D case.

4.3.5 Summary of Advection-Dispersion Results. The preceding sections assumed the B-52H aircraft, which has a TF33-3 engine that gives 0.21 lb/hr of output fuel at idle. Of course, this is a conservative case giving near worst-case results. If we perform the same analysis with a different B-52 model (different engine type) and the B-1, we would see a smaller source term and therefore shorter “critical” distance, or the distance at which the aerosol airborne concentration goes below the hydrocarbon standard. The following table (4.9) summarizes these differing critical distances for the three different aircraft (output at idle; critical distances for both continuous and instantaneous results):

Table 4.9: Critical Distances for Three Different Engine Types

Aircraft Type	Engine Type	# of Engines	Output (lb/hr)	Crit Dist; Cont	Crit Dist; Inst
B-52 H	TF33-3	8	0.21	59 (case A-B)	106 (case A-B)
	TF33-3	8	0.21	47 (case B-C)	157 (case B-C)
	TF33-3	8	0.21	56 (case C-D)	249 (case C-D)
B-52 G	J57-43	8	0.14	47 (case A-B)	91 (case A-B)
	J57-43	8	0.14	38 (case B-C)	135 (case B-C)
	J57-43	8	0.14	45 (case C-D)	214 (case C-D)
B-1	F101-102	4	0.04	16 (case A-B)	45 (case A-B)
	F101-102	4	0.04	13 (case B-C)	66 (case B-C)
	F101-102	4	0.04	15 (case C-D)	104 (case C-D)

As we see from Table 4.9, we observe a decrease in the critical distance when we have a different B-52 model and engine type. The significant decrease in critical distance occurs when we observe the B-1, with its decrease in source term and # of engines from the B-52. It should be noted that the "instantaneous" numbers for the B-1 may be wrong because we are assuming a 10-minute cold startup, when in fact the more efficient B-1 engine type may not need 10 minutes before combustion occurs. Regardless, the results show that the B-52 is indeed the area of concern for downwind concentration.

Thus far, we have assumed no evaporation, which causes our results to be on the conservative side. When we incorporate evaporation into our model, we will notice a greater decrease in airborne mass and therefore a greater decrease in airborne concentration with time.

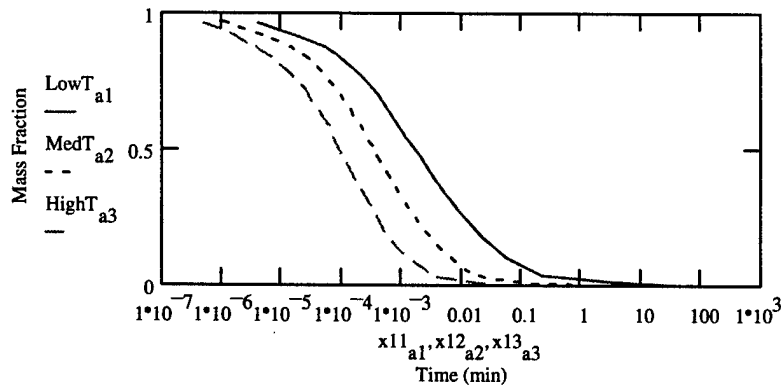
4.4 Evaporation and Settling Combined.

4.4.1 Evaporation of JP-4 Droplets. Evaporation will have an important impact on our results depending on the temperature and the volatility of the fuel in question. By previously neglecting evaporation in our model, we arrived at very conservative results for the downwind concentrations of the fuel aerosol.

By employing Clewell's evaporation model to arrive at our evaporation analysis, we notice some interesting characteristics. First, as Lowell concluded (17:2), we do indeed see a sizable difference in percent evaporation as we vary the temperature from -20°C to 20°C. Moreover, the larger droplets will experience less mass loss with time because as we increase the droplet size, we increase the volume by the radius cubed (versus radius squared as the evaporation formula tells us). We look at the evaporation of droplets from

7.5 to 115 μm (95% of the distribution) so we cover more than ± 2 sigma of the mass distribution. Figure 4.11 shows the evaporation of the 7.5 μm droplet at -20°C (LowT), 0°C (MedT), and 20°C (HighT):

Figure 4.11: Evaporation of 7.5 μm JP-4 Droplet



As expected, we see an increase in percent evaporation (mass percentage remaining is the y-axis) with time when we increase temperature. The leftmost case is the 20°C case, while the rightmost case is the -20°C case. Particular values of percent mass remaining were obtained (see Table 4.10) for a particular time and for each diameter. For the above case, at $.15 \times 10^{-3}$ minutes, we see the fraction of mass remaining to be .80, .63, and .41 for -20 , 0 and 20 degrees respectively. We also see that for all cases, mass remaining goes to approximately zero relatively quickly (less than 1 minute for all cases). Table 4.10 below shows the mass differences at particular times for the different droplet cases:

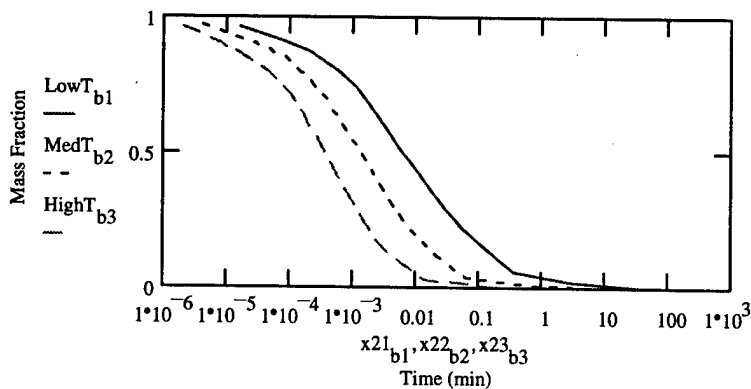
Table 4.10: Mass Remaining at Various Times for JP-4 Droplets:

Diameter (μm)	Time (Minutes)	-20°C	0°C	20°C
7.5	.15E-3	.80	.63	.41
15	.11E-2	.74	.52	.30
25	.20E-2	.78	.59	.35
35	.24E-1	.54	.30	.11
45	.28E-2	.85	.71	.51
55	.12E-1	.74	.53	.32
65	.14E-1	.76	.56	.34
75	.43E-3	.65	.42	.20
85	.13E+0	.52	.28	.10
95	.11E-1	.84	.69	.50
105	.11E-1	.85	.71	.53
115	.11E-1	.86	.72	.56

The average difference of evaporation for the given times above is .18 from -20°C to 0°C, and .20 from 0°C to 20°C. Figures 4.11 to 4.22 demonstrate this trend of an approximately constant evaporation difference with time.

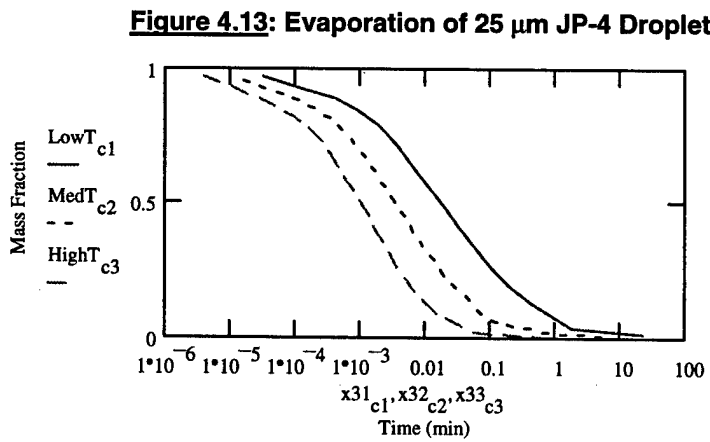
Figure 4.12 shows the evaporation for the 15 μm drop:

Figure 4.12: Evaporation of 15 μm JP-4 Droplet



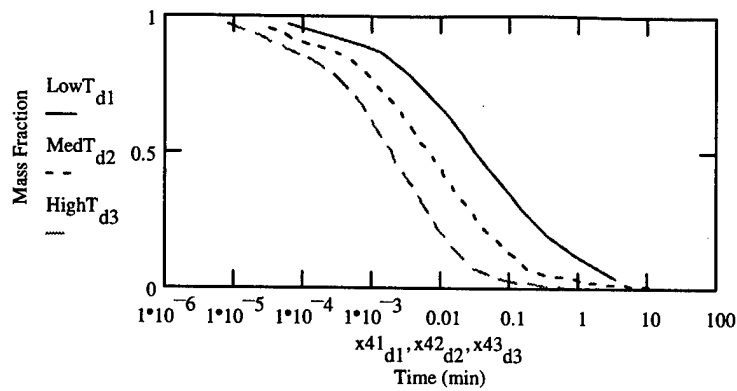
For this case, at $.11 \times 10^{-2}$ minutes (Table 4.10), we have .74, .52, and .30 as the fraction of mass remaining for the three temperature cases. We see that for the two cases thus far, the mass remaining difference for the cases has been around .20 for a given time (and this difference is approximately constant from Figures 4.11 and 4.12).

Figure 4.13 shows the evaporation of the 25 μm droplet:



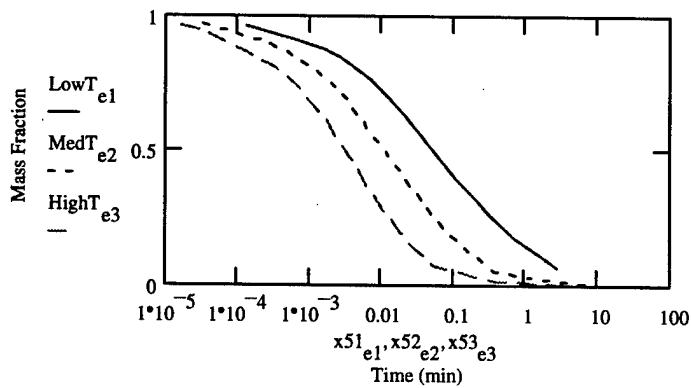
We see that for the 25 μm case, we still retain a small percentage of mass for the -20°C case even after 10 minutes. This again points to the fact we notice smaller mass percentage loss with time as we increase our droplet size. Figure 4.14 shows the evaporation of the 35 μm droplet:

Figure 4.14: Evaporation of 35 μm JP-4 Droplet



We see for the -20°C case, the droplet will reach ground before the droplet is completely evaporated, while the other two cases will still completely evaporate in the air. Figure 4.15 shows the 45 μm droplet evaporation:

Figure 4.15: Evaporation of 45 μm JP-4 Droplet



Figures 4.16 through 4.22 show the evaporation of the 55 through 115 μm droplets:

Figure 4.16: Evaporation of 55 μm JP-4 Droplet

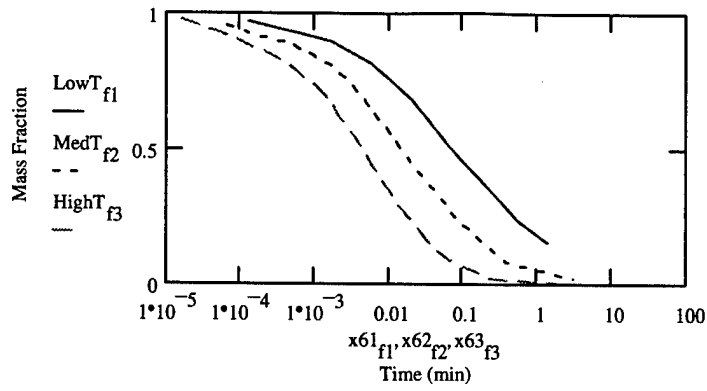


Figure 4.17: Evaporation of 65 μm JP-4 Droplet

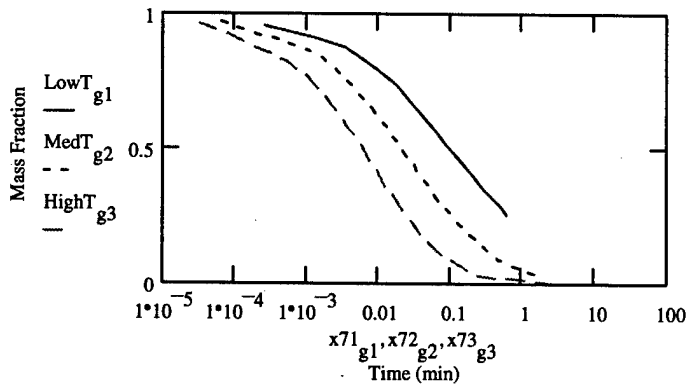


Figure 4.18: Evaporation of 75 μm JP-4 Droplet

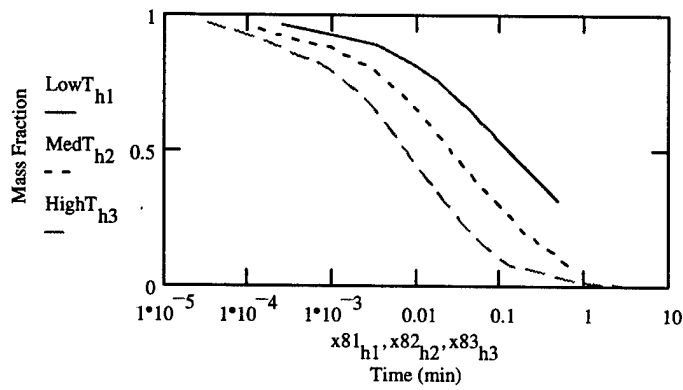


Figure 4.19: Evaporation of 85 μm JP-4 Droplet

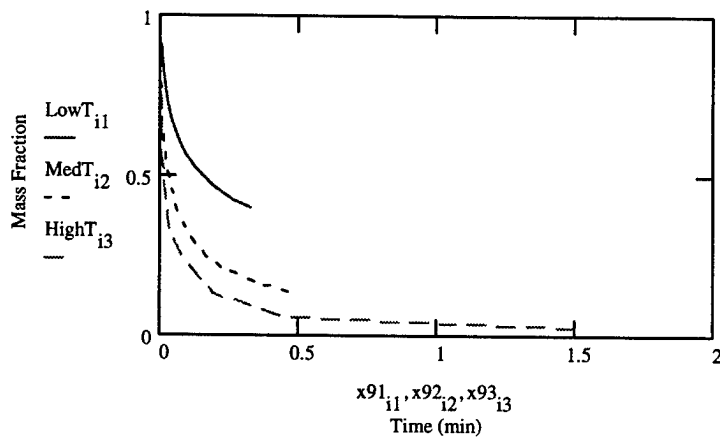


Figure 4.20: Evaporation of 95 μm JP-4 Droplet

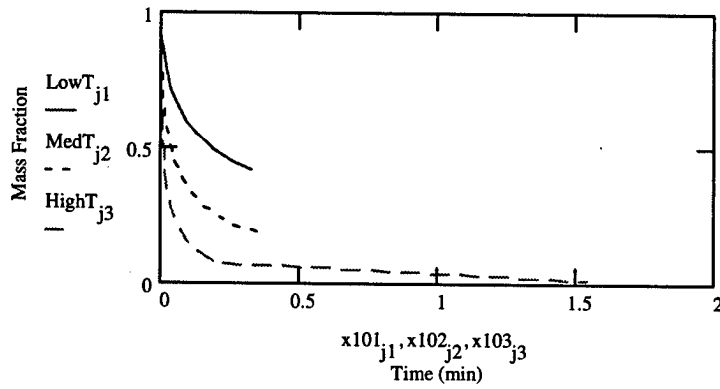


Figure 4.21: Evaporation of 105 μm JP-4 Droplet

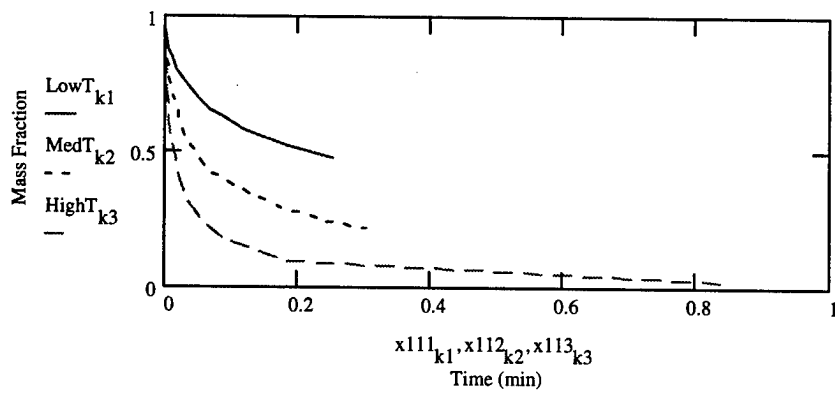
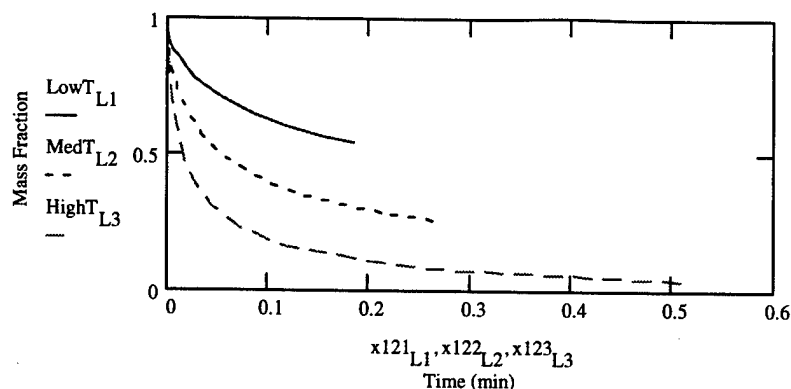


Figure 4.22: Evaporation of 115 μm JP-4 Droplet



As we see from the previous cases for droplets with radii from 45 μm to 115 μm , the trend of more aerosol mass remaining in the air and reaching the ground with time continues. For the 85 μm case, the evaporation is sufficiently slow that we can use a normal scale on both axes for display, whereas for the smaller droplets there is so much evaporation that the figures need a log scale for time (x-axis). For the 115 μm case, we see that in all three cases the droplet falls to the ground relatively quickly. At 20°C, time to ground is longer because the greater evaporation (due to temperature) decreases the droplet size to a greater extent, prolonging its airborne time. Once again with the 115 μm case, we can more clearly see that the mass remaining difference for the three temperature cases is approximately 0.2. But even at the 115 μm case, we see significant evaporation occurring by the time the drop reaches the ground. This compelling evidence shows the important effect evaporation will have on our final results (even though we may surmise that evaporation will not be as significant for JP-8 droplets).

At this point, it becomes important to show the total amount of JP-4 that reaches the ground at various temperatures. Table 4.11 below shows the total amount of JP-4 reaching the ground at 0°C:

Table 4.11: Amount of JP-4 Reaching Ground When Temperature is 0°C

Diameter	% of Distribution	Time to Ground	Amt Remaining	Total to Ground
7.5	6.7	evaporated in air	0	0
15	19.7	evaporated in air	0	0
25	18.7	evaporated in air	0	0
35	14.2	173 min	.0014	1.99E-4
45	10.3	11.6 min	.0017	1.75E-4
55	7.5	3.05 min	.022	1.65E-4
65	5.4	1.81 min	.029	1.57E-4
75	4.0	46 sec	.068	2.72E-3
85	2.9	30 sec	.133	3.86E-3
95	2.2	23 sec	.173	3.81E-3
105	1.7	18 sec	.219	3.72E-3
115	1.3	16 sec	.254	3.30E-3
125	1.0	14 sec	.315	3.15E-3
135	0.79	12 sec	.332	2.62E-3
145	0.63	10 sec	.374	2.36E-3
175	1.7	6 sec	.492	8.36E-3
225	0.65	4 sec	.618	4.02E-3
275	0.28	3 sec	.714	<u>2.0E-3</u>
				0.0435

By similar treatment, we find that the total amount of JP-4 reaching the ground at -20°C is **.123** and for 20°C, **.0116**, representing a sizable gap in evaporation of JP-4 from -20°C to 20°C (from 12.3% to 1.16%).

4.4.2 Evaporation of JP-8 Droplets. Evaporation of JP-8 fuel droplets is very similar to that of the JP-4 droplets; however, we observe a lesser degree of evaporation due to the higher density and less volatility of the JP-8 droplet. Figures 4.23 through 4.29 below

show the evaporation of JP-8 droplets from 7.5 to 65 μm ; from this sample we see the upward trend of the amount (percentage) of mass remaining in the droplet, as we did with the JP-4 droplets:

Figure 4.23: Evaporation of JP-8, 7.5 μm

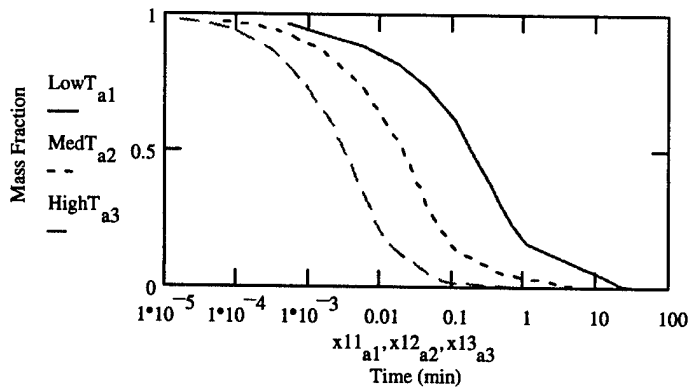


Figure 4.24: Evaporation of JP-8, 15 μm

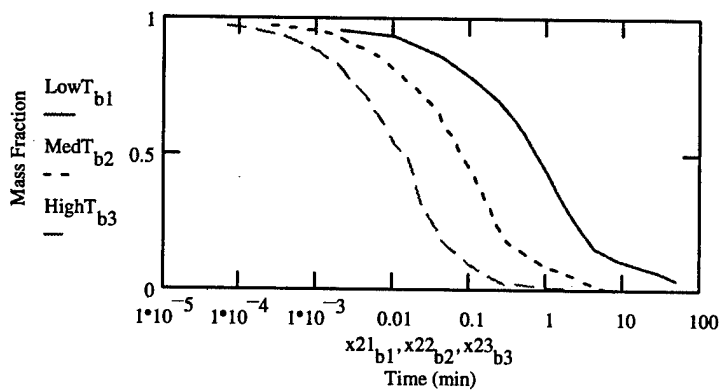


Figure 4.25: Evaporation of JP-8, 25 μm

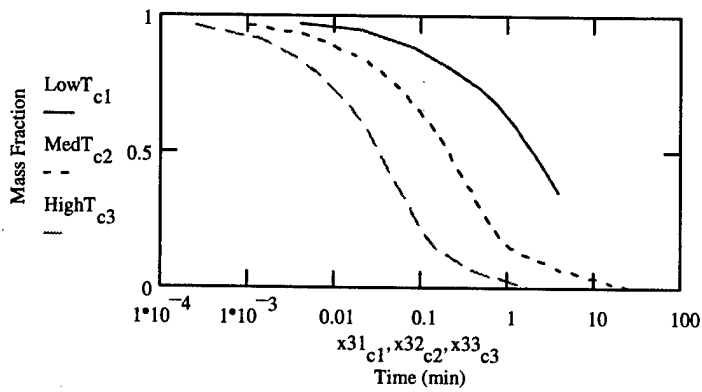


Figure 4.26: Evaporation of JP-8, 35 μm

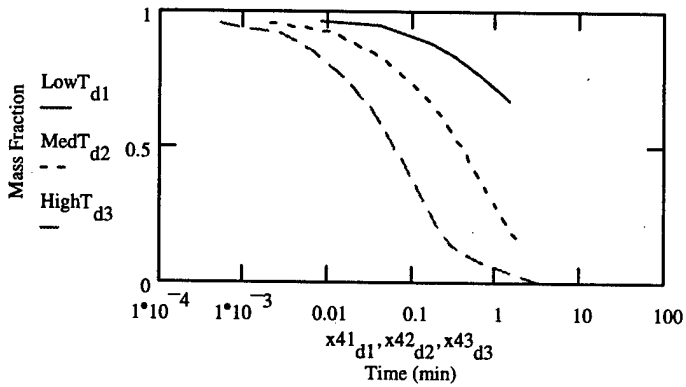


Figure 4.27: Evaporation of JP-8, 45 μm

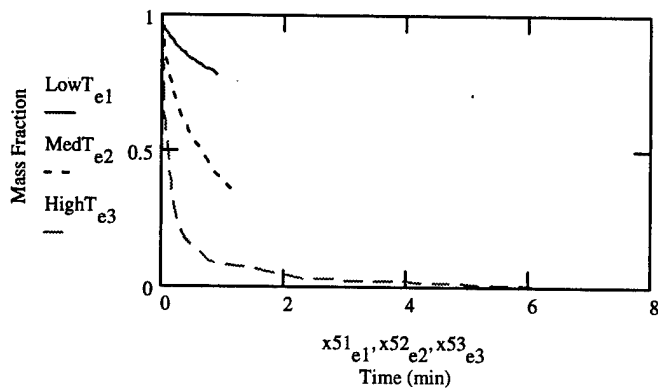


Figure 4.28: Evaporation of JP-8, 55 μm

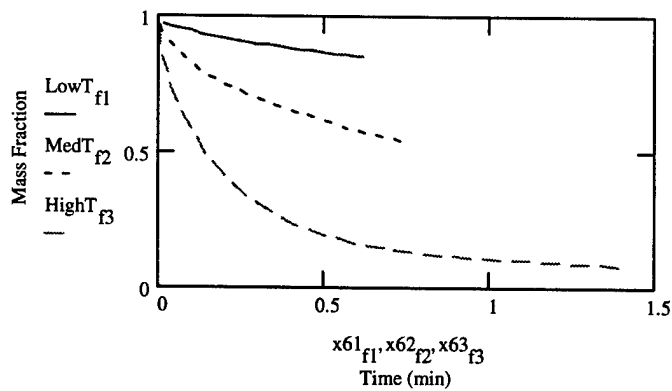
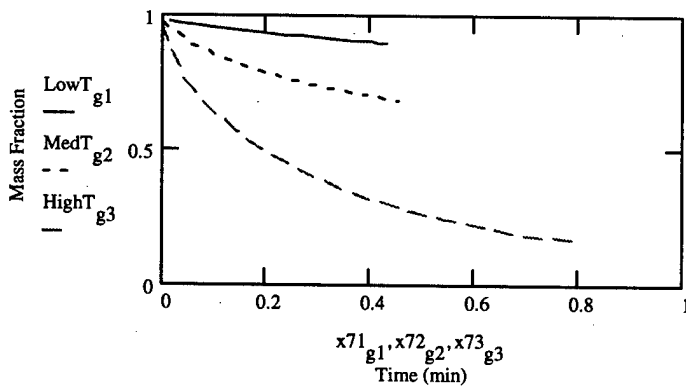


Figure 4.29: Evaporation of JP-8, 65 μm



The above graphs once again show the evaporation (mass proportion remaining, y-axis) versus time (in minutes, x-axis), with the descending mass proportion remaining going from -20°C , 0°C , to 20°C degrees, respectively. With $7.5 \mu\text{m}$, we see that even after ten minutes, the remaining amount of droplet is still airborne (for the -20 degree case) due to the low Stokes' velocity for this small droplet size. The other temperature cases show a greater amount of evaporation with time. For a droplet with a diameter of $65 \mu\text{m}$, we see that the droplets do not remain airborne nearly as long due to the greater Stokes' velocities. Table 4.12 below shows the mass remaining for the droplets at the three temperature cases and at various times:

Table 4.12: JP-8 Evaporation Cases for Various Temperatures

Diameter	Time (min)	-20°C	0°C	20°C
7.5	0.15E-1	0.84	0.56	0.13
15	0.20E-1	0.91	0.74	0.39
25	0.34E-1	0.93	0.79	0.49
35	0.10E+1	0.91	0.73	0.37
45	0.29E+0	0.88	0.65	0.22
55	0.60E+0	0.85	0.58	0.16
65	0.25E+0	0.93	0.76	0.44

For JP-8 droplets, we find that the average mass remaining differences (for the times indicated in Table 4.12) are **.20** for a temperature change from -20°C to 0°C and **.37** from 0°C to 20°C. Figures 4.28 and 4.29 more clearly convey this sizable difference for temperature changes from -20°C and 0°C to 0°C and 20°C in terms of evaporation.

As with the JP-4, we are interested in the amount of JP-8 reaching the ground for the various temperature cases. Table 4.13 shows the amount of JP-8 reaching the ground:

Table 4.13: Amount of JP-8 Reaching Ground When Temperature is 0°C

Diameter	% of Distribution	Time to Ground	Amt Remaining	Total to Ground
7.5	6.7	evaporated in air	0	0
15	19.7	evaporated in air	0	0
25	18.7	178 min	.0011	2.06E-4
35	14.2	2.20 min	.141	.0200
45	10.3	1.23 min	.341	.0351
55	7.5	44 sec	.541	.0406
65	5.4	30 sec	.682	.0368
75	4.0	22 sec	.775	.031
85	2.9	17 sec	.799	.0232
95	2.2	14 sec	.831	.0183
105	1.7	11 sec	.873	.0148
115	1.3	10 sec	.887	.0115
125	1.0	8 sec	.897	8.97E-3
135	0.79	7 sec	.932	7.36E-3
145	0.63	6 sec	.938	5.91E-3
175	1.7	4 sec	.951	.0162
225	0.65	2.5 sec	.982	6.38E-3
275	0.28	1.5 sec	.986	<u>2.76E-3</u>
				0.279

By similar treatment, for -20°C we have **.526** as the mass fraction reaching the ground and for 20°C we have **.112** reaching the ground. For JP-8, we therefore see a range from 52.6% to 11.2% reaching the ground as we change ground temperatures from -20°C to 20°C .

4.4.3 JP-4 and JP-8 Constituents. As we have examined the droplet evaporation for JP-4 and JP-8, we must also observe the individual component evaporation for both JP-4 (33 components) and JP-8 (27 components). As the droplet moves through the air, the more volatile components of either fuel will evaporate more readily, causing the density of what remains of the droplet to actually increase. Eventually, the droplet will be made up of entirely the less volatile components. The components for this study have been grouped into carbon groups, or by the number of carbon atoms in a particular component. The appendix shows the breakdown for both fuels in terms of the number of carbon atoms each component contains. Figures 4.30 and 4.31 below show constituent evaporation with time (in minutes) for JP-4, taking a representative droplet size of $35\text{ }\mu\text{m}$ (which is approximately at the 50% point in the droplet size distribution) and 0°C :

Figure 4.30: Evaporation of JP-4 Constituents C6-C9, 0°C and 35 μm

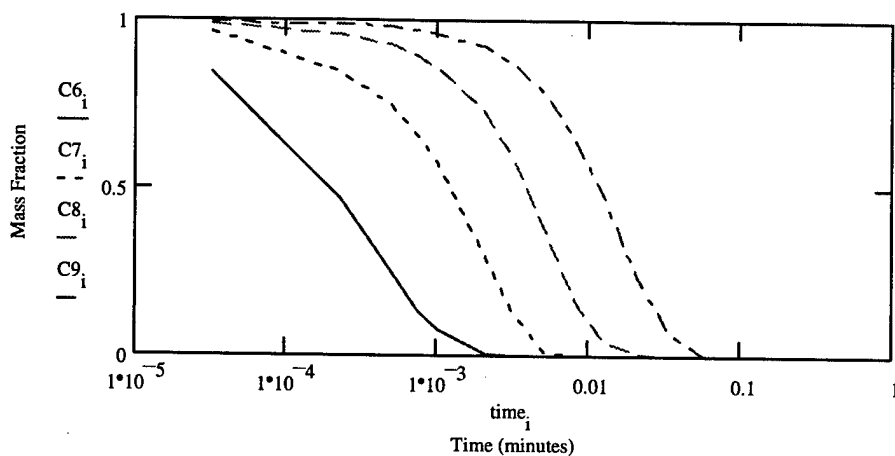
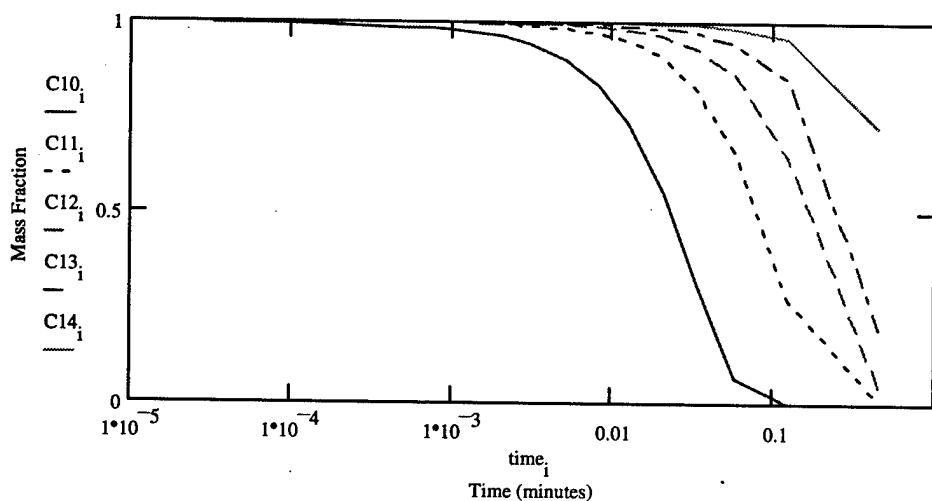


Figure 4.31: Evaporation of JP-4 Constituents C10-C14, 0°C and 35 μm



The evaporation of JP-4 slows down with increasing carbon atoms: the C6 group (Fig 4.30) evaporates relatively quickly while the C14 group (Fig 4.31) evaporates relatively slowly. At the half minute mark, the drop in made up mostly of the C14 group. Table 4.14 shows the constituent evaporation with time for the JP-4 droplet, 35 μm and 0°C:

Table 4.14: JP-4 Constituents (Remaining Proportions) at 0°C for 35 μm

Time, m	C6	C7	C8	C9	C10	C11	C12	C13	C14
.326E-4	.843	.963	.991	.996	.994	1.0	1.0	1.0	1.0
.977E-4	.630	.900	.972	.990	.993	1.0	1.0	1.0	1.0
.488E-3	.248	.749	.926	.980	.986	.999	.998	.999	1.0
.00101	.0746	.569	.860	.960	.980	.999	.998	.999	1.0
.00309	0	.135	.60	.875	.945	.992	.996	.995	1.0
.0083	0	0	.162	.647	.832	.971	.988	.994	.999
.0208	0	0	.00341	.240	.551	.905	.963	.983	.996
.0583	0	0	0	.00128	.0664	.664	.863	.943	.985
.125	0	0	0	0	0	.269	.647	.847	.957
.458	0	0	0	0	0	.0127	.0456	.197	.722

Figures 4.32 and 4.33 below show the constituent evaporation of JP-8. The evaporation as a whole is not as pronounced for the JP-8, but the constituent evaporation is similar to that of the JP-4 case:

Figure 4.32: Evaporation of JP-8 Constituents C8-C11, 0°C and 35 μm

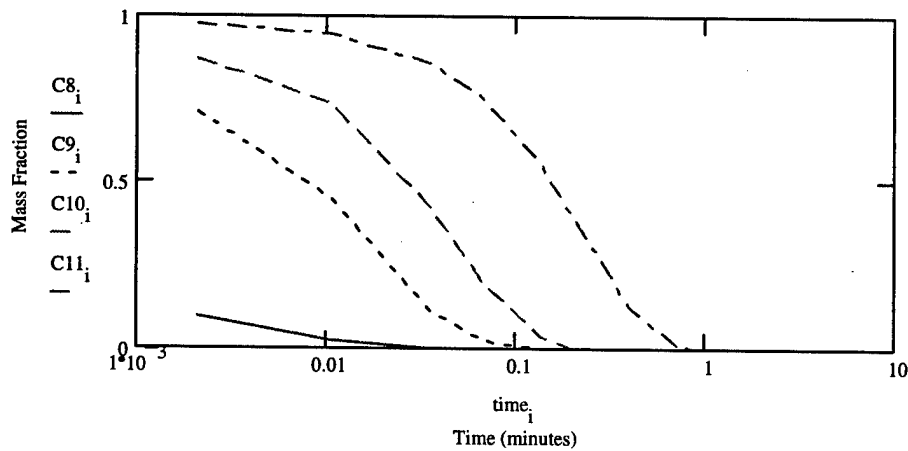
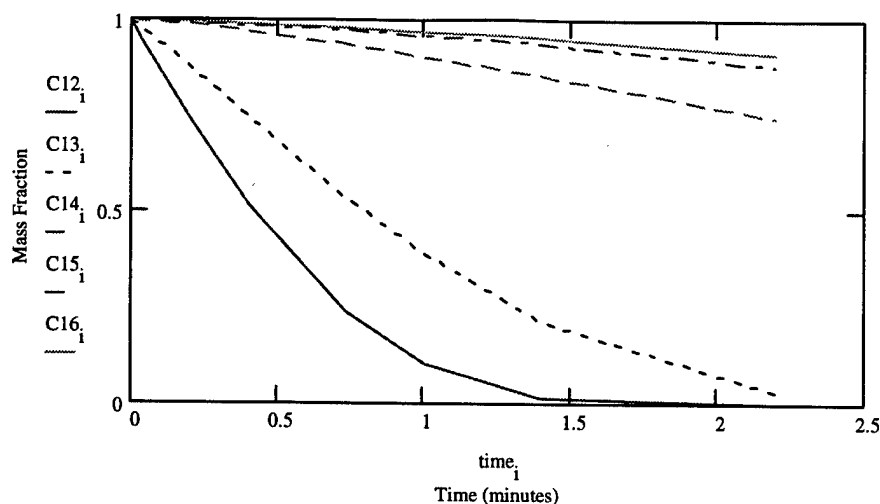


Figure 4.33: Evaporation of JP-8 Constituents C12-C16, 0°C and 35 μm



With the JP-8, we see a relatively small amount of evaporation of the C14, C15, and C16 constituents after 2 minutes, while the C8-C13 are virtually gone after the two minute mark. Table 4.15 below summarizes the constituent evaporation of the 35 μm JP-8 droplet at 0°C:

Table 4.15: JP-8 Constituents (Remaining Proportions) at 0°C for 35 μm

Time, m	C8	C9	C10	C11	C12	C13	C14	C15	C16
.00208	.0978	.707	.870	.975	.989	.995	1.0	1.0	1.0
.0104	.0242	.453	.738	.949	.980	.992	1.0	1.0	1.0
.0354	0	.111	.421	.860	.949	.978	.997	1.0	.999
.0688	0	.0264	.196	.750	.907	.959	.997	.998	.999
.135	0	0	.0337	.555	.823	.917	.992	.995	.997
.202	0	0	0	.401	.741	.875	.987	.993	.996
.402	0	0	0	.125	.516	.744	.969	.986	.991
.735	0	0	0	.007	.237	.538	.935	.972	.981
1.00	0	0	0	0	.106	.390	.903	.958	.971
1.40	0	0	0	0	.0142	.215	.852	.936	.954
2.20	0	0	0	0	0	.0299	.743	.882	.913

4.4.4 Total Evaporation With Time of JP-4 and JP-8. The preceding results for individual droplets enables us to determine the total evaporation with time of JP-4 at -20°C, 0°C, and 20°C and JP-8 at -20°C, 0°C, and 20°C. For the time intervals of 1, 2, 3, 4, 5, 10, 20, 30, 40 and 50 seconds, and 1, 2, 3, 4, and 5 minutes, it is necessary to determine the amount remaining of each of the droplets in our distribution (from Table 4.1), and then to add up these quantities by the corresponding percent masses they represent in the total distribution. By doing this, we arrive at a total amount remaining of either JP-4 or JP-8. Tables 4.16 through 4.21 below display the total evaporation of our six cases (two fuels types times three temperature cases):

Table 4.16: Evaporation of JP-4 at -20°C

Time	Amount Remaining
1 sec	.566
2 sec	.477
3 sec	.424
4 sec	.381
5 sec	.358
10 sec	.257
20 sec	.156
30 sec	.127
40 sec	.0951
50 sec	.0717
1 min	.0556
2 min	.0316
3 min	.0177
4 min	.0102
5 min	.0091

Table 4.17: Evaporation of JP-8 at -20°C

Time	Amount Remaining
1 sec	.945
2 sec	.923
3 sec	.908
4 sec	.888
5 sec	.833
10 sec	.793
20 sec	.658
30 sec	.533
40 sec	.440
50 sec	.415
1 min	.314
2 min	.157
3 min	.122
4 min	.107
5 min	.0346

Table 4.18: Evaporation of JP-4 at 0°C

Time	Amount Remaining
1 sec	.353
2 sec	.265
3 sec	.218
4 sec	.188
5 sec	.160
10 sec	.107
20 sec	.0652
30 sec	.0362
40 sec	.0262
50 sec	.0195
1 min	.0140
2 min	.0108
3 min	.0065
4 min	.0038
5 min	.0027

Table 4.19: Evaporation of JP-8 at 0°C

Time	Amount Remaining
1 sec	.855
2 sec	.795
3 sec	.745
4 sec	.711
5 sec	.663
10 sec	.543
20 sec	.372
30 sec	.283
40 sec	.212
50 sec	.143
1 min	.123
2 min	.0504
3 min	.0190
4 min	.0148
5 min	.0098

Table 4.20: Evaporation of JP-4 at 20°C

Time	Amount Remaining
1 sec	.176
2 sec	.116
3 sec	.0858
4 sec	.0649
5 sec	.0544
10 sec	.0265
20 sec	.0130
30 sec	.0065
40 sec	.0033
50 sec	.0016
1 min	.0008

Table 4.21: Evaporation of JP-8 at 20°C

Time	Amount Remaining
1 sec	.668
2 sec	.558
3 sec	.480
4 sec	.432
5 sec	.379
10 sec	.251
20 sec	.130
30 sec	.065
40 sec	.033
50 sec	.016
1 min	.008

With these tables above, we again see the trend of increased evaporation when we move from JP-8 to JP-4 and from -20°C to 20°C. For the 20°C cases for both JP-4 and JP-8, over 99% of the fuel is evaporated in 1 minute. These results combine settling and evaporation since we are only looking at (in tables 4.16 to 4.21) airborne fuel; once it hits the ground, it is neglected. These results therefore may combine with the advection-dispersion results (with the same time intervals) to arrive at the total airborne concentration combining all the physical phenomena in our study.

4.4.5 Determination of Accurate Source Terms. Before we continue with the total airborne concentration analysis, we must re-compute the source terms for the instantaneous case, taking into account the effects of evaporation (whereas previously we approximated the terms only looking at settling). Table 4.22 below shows the computation of the source terms for JP-4 and JP-8 at 0°C:

Table 4.22: Determination of the Source Term for JP-4 and JP-8 at 0°C

Time	Fuel Emit, μg	JP-4 Evap	JP-4 Left, μg	JP-8 Evap	JP-8 Left, μg
1 sec	211866	.353	74789	.855	181145
2 sec	211866	.265	56144	.795	168434
3 sec	211866	.218	46187	.745	157840
4 sec	211866	.188	39831	.711	150637
5 sec	211866	.160	33899	.663	140467
10 sec	1059330	.107	113348	.543	575216
20 sec	2118660	.0652	138137	.372	788142
30 sec	2118660	.0362	76695	.283	599581
40 sec	2118660	.0262	55509	.212	449156
50 sec	2118660	.0195	41314	.143	302968
1 min	2118660	.0140	29662	.123	260595
2 min	12711960	.0108	137289	.0504	640683
3 min	12711960	.0065	82628	.0190	241527
4 min	12711960	.0038	48306	.0148	188137
5 min	12711960	.0027	<u>34322</u>	.0098	<u>124577</u>
			1008058		4969105

The above numbers were figured by assuming the emission of our most critical B-52 case (the B-52H), which emits 211866 μg of fuel per second. Then, with the evaporation values from tables 4.16 and 4.17, we arrive at the amount (approximately) of fuel remaining in our fuel cloud. By similar computation, we arrive at source terms for JP-4 at -20°C and 20°C, **2682435** and **186781** μg and JP-8 at -20°C and 20°C, **12139498** and **1333061** μg .

4.5 Combined Settling / Advection / Dispersion / Evaporation of JP-4 and JP-8.

In sections 4.2 through 4.4, we developed the individual aspects of settling, advection and dispersion, and evaporation of the two fuels of interest (although the evaporation section was based on a Clewell model that combines settling and evaporation). Here, we are interested in combining the aforementioned sections into one overall section, with final conclusions coming from this total analysis.

We are interested in looking at the behavior of the fuel when in the condition A-B because, due to the low wind velocity (at ground level), the higher concentrations will be around for a longer period of time. For stability classes B-C and C-D, the wind velocities are higher and therefore disperse the aerosol more quickly in the x-direction, even though the aerosol concentration will not fall below the standard until further downstream because these cases are more stable. Hence, it becomes a trade-off between time and distance; stability class A-B is more time critical while stability class C-D is more distance critical. The following figures, 4.34 through 4.45, combine the results from tables 4.3 and 4.6 (continuous and instantaneous case for stability class A-B) and tables 4.16 through 4.21 (total evaporation of the two fuels at the three temperatures):

Figure 4.34: JP-4 Evap/Disp at -20°C ($\mu\text{g}/\text{m}^3$), Contin Case (A-B)

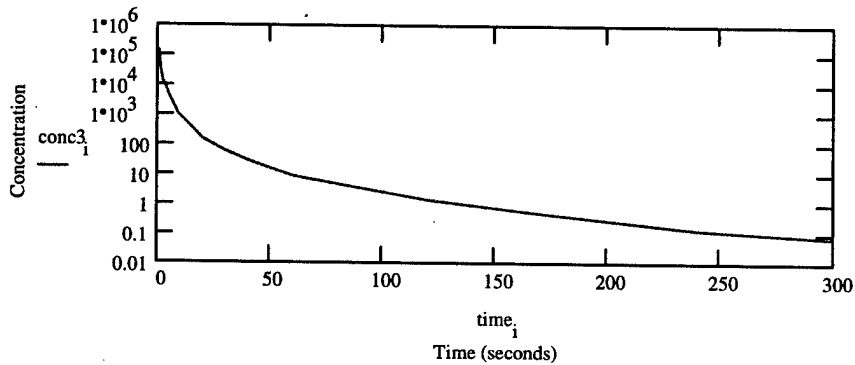


Figure 4.35: JP-4 Evap/Disp at -20°C ($\mu\text{g}/\text{m}^3$), Inst Case (A-B)

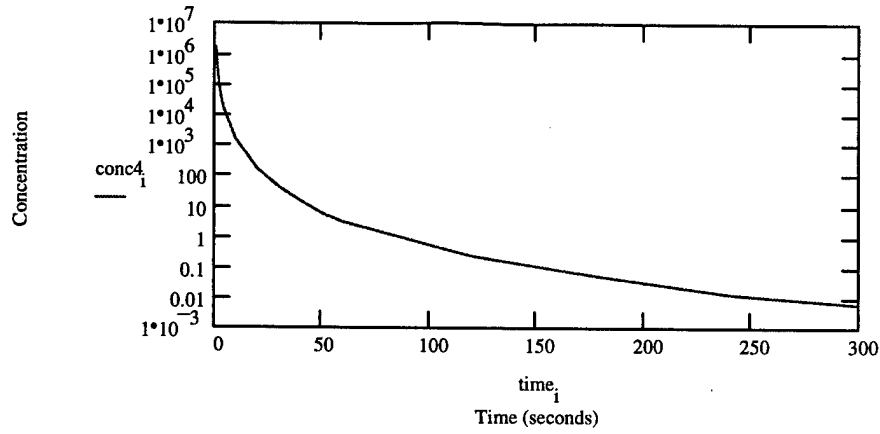


Figure 4.36: JP-4 Evap/Disp at 0°C ($\mu\text{g}/\text{m}^3$), Contin Case (A-B)

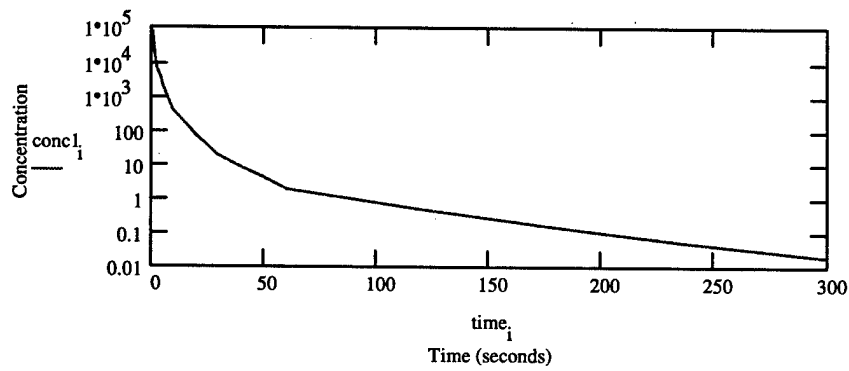


Figure 4.37: JP-4 Evap/Disp at 0°C ($\mu\text{g}/\text{m}^3$), Inst Case (A-B)

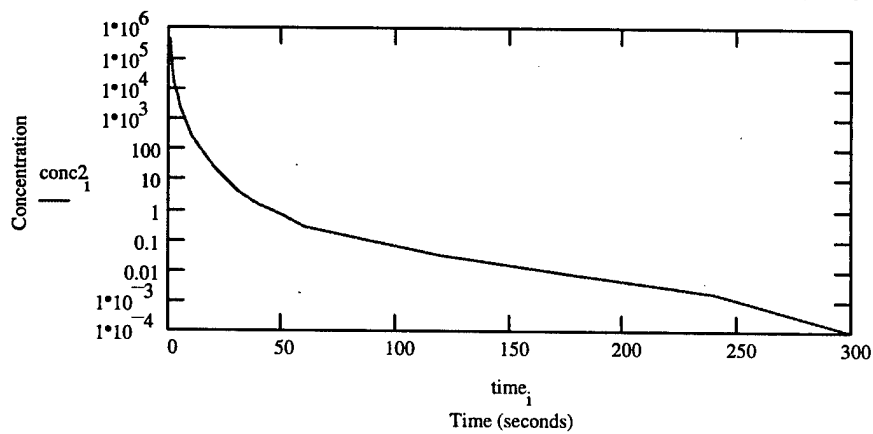


Figure 4.38: JP-4 Evap/Disp at 20°C ($\mu\text{g}/\text{m}^3$), Contin Case (A-B)

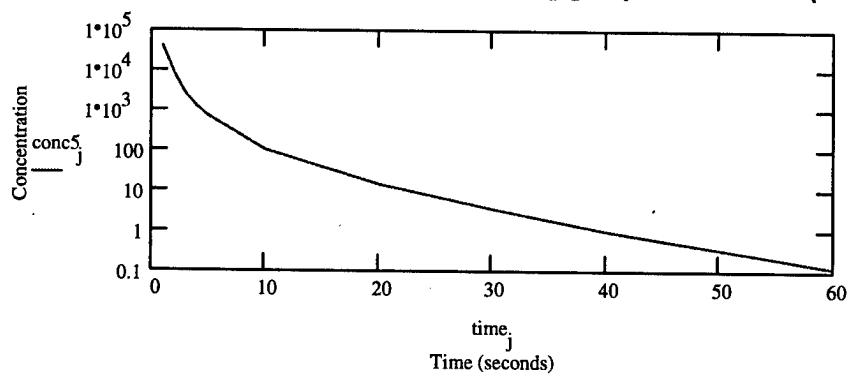


Figure 4.39: JP-4 Evap/Disp at 20°C ($\mu\text{g}/\text{m}^3$), Inst Case (A-B)

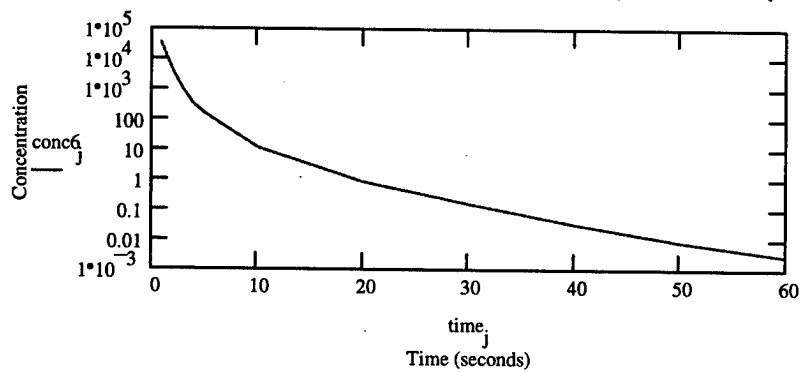


Figure 4.40: JP-8 Evap/Disp at -20°C ($\mu\text{g}/\text{m}^3$), Contin Case (A-B)

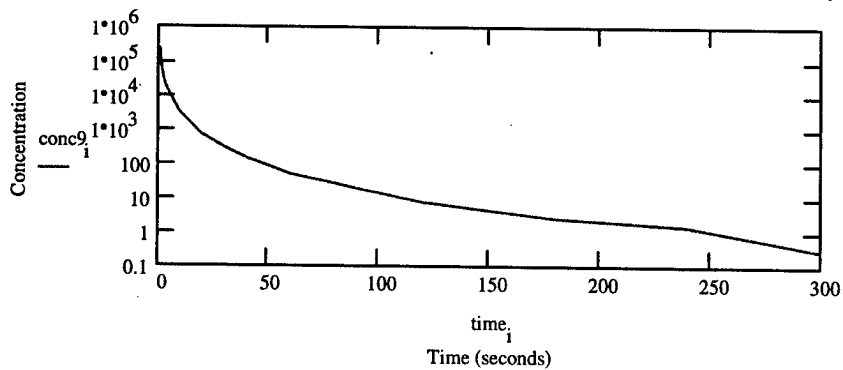


Figure 4.41: JP-8 Evap/Disp at -20°C ($\mu\text{g}/\text{m}^3$), Inst Case (A-B)

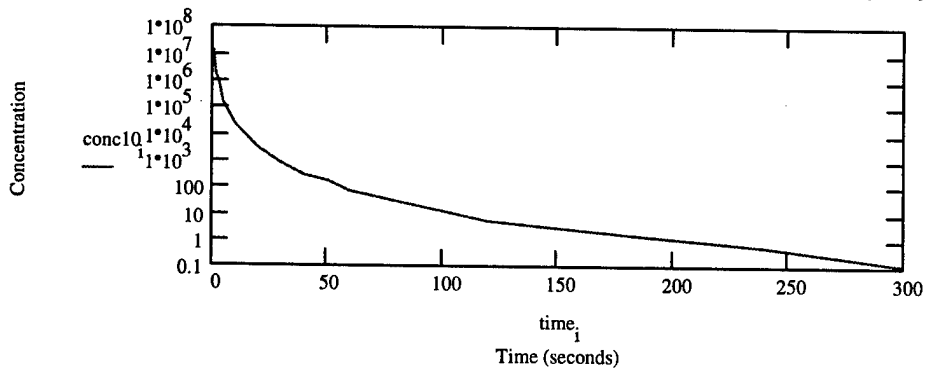


Figure 4.42: JP-8 Evap/Disp at 0°C ($\mu\text{g}/\text{m}^3$), Contin Case (A-B)

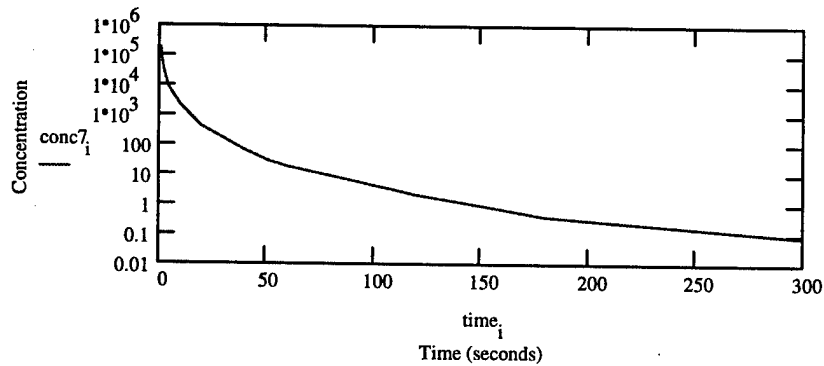


Figure 4.43: JP-8 Evap/Disp at 0°C ($\mu\text{g}/\text{m}^3$), Inst Case (A-B)

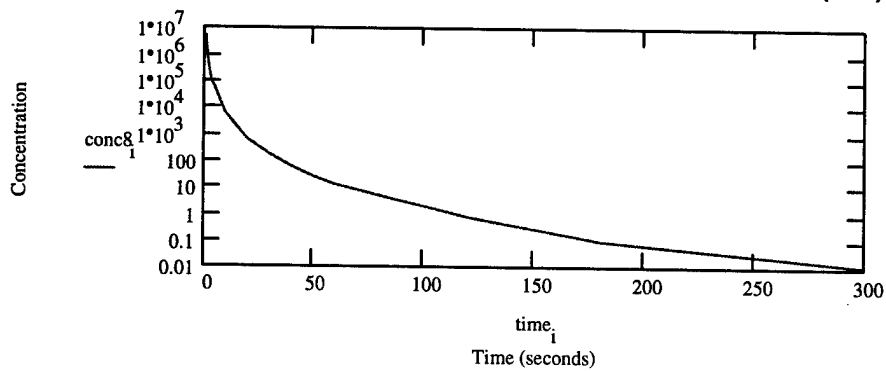


Figure 4.44: JP-8 Evap/Disp at 20°C ($\mu\text{g}/\text{m}^3$), Contin Case (A-B)

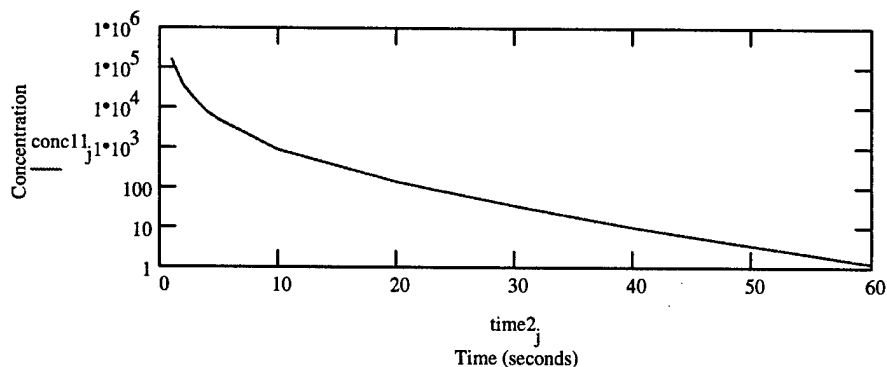
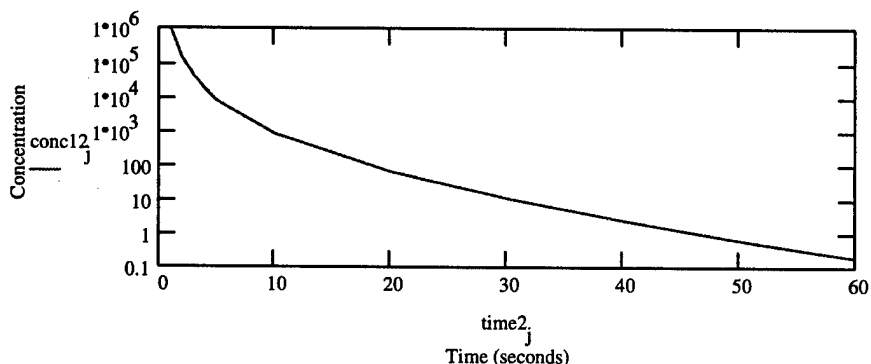


Figure 4.45: JP-8 Evap/Disp at 20C ($\mu\text{g}/\text{m}^3$), Inst Case (A-B)



Again, we see with Figures 4.34 through 4.45 behavior that corroborates our previous advection-dispersion and evaporation findings. The evaporation just accentuates the relatively quick decrease in concentration with time of our aerosol (although this rate of decrease is affected by the temperature and fuel type as shown). Figures 4.34 through 4.45 depict concentration ($\mu\text{g}/\text{m}^3$) versus time (seconds), unlike the previously displayed advection-dispersion figures (4.5 through 4.10) depicting distance versus time. With the

A-B case, since we assume 1 m/s, the x-axis quantities turn out to be the same; however, the B-C and C-D cases would be converted from distance to time to include the evaporation data, which is in terms of time.

Tables 4.23 through 4.28 combine the advection-dispersion data without evaporation (Figures 4.5-4.10) and the total evaporation data of Tables 4.16-4.21. While Figures 4.34-4.45 display the data for stability class A-B, Tables 4.23-4.28 include the data for all three stability classes.

Table 4.23: Concentration ($\mu\text{g}/\text{m}^3$) Versus Time for JP-4 at -20°C

Time	A-B, Cont	B-C, Cont	C-D, Cont	A-B, Inst	B-C, Inst	C-D, Inst
1 sec	129430	12239	6703	1702481	257244	224326
2 sec	31586	2987	1636	223574	33782	29459
3 sec	13599	1286	704	66987	10122	8827
4 sec	7306	691	378	27827	4205	3667
5 sec	4606	436	239	14372	2172	1894
10 sec	958	90.5	49.6	1608	243	212
20 sec	168	15.9	8.72	152	23.0	20.0
30 sec	66.4	6.28	3.44	41.7	6.31	5.50
40 sec	29.7	2.81	1.54	14.4	2.18	1.90
50 sec	15.0	1.42	0.78	5.99	0.90	0.78
1 min	8.41	0.80	0.44	2.85	0.43	0.38
2 min	1.38	0.13	0.07	0.25	0.04	0.03
3 min	0.38	0.04	0.02	0.05	0.007	0.006
4 min	0.13	0.01	0.007	0.01	0.002	0.002
5 min	0.08	0.007	0.004	0.006	0.001	0.0008

Table 4.24: Concentration ($\mu\text{g}/\text{m}^3$) Versus Time for JP-4 at 0°C

Time	A-B, Cont	B-C, Cont	C-D, Cont	A-B, Inst	B-C, Inst	C-D, Inst
1 sec	80772	7633	4180	399022	60292	52577
2 sec	17548	1659	909	46677	7053	6150
3 sec	6992	661	362	12943	1956	1705
4 sec	3605	341	187	5160	780	680
5 sec	2059	195	107	2414	365	318
10 sec	399	37.7	20.6	252	38.0	33.1
20 sec	70.3	6.65	3.64	23.9	3.61	3.15
30 sec	18.9	1.79	0.98	4.47	0.68	0.59
40 sec	8.19	0.77	0.42	1.50	0.23	0.20
50 sec	4.09	0.39	0.21	0.61	0.09	0.08
1 min	2.12	0.20	0.11	0.27	0.04	0.04
2 min	0.47	0.04	0.02	0.03	0.005	0.004
3 min	0.14	0.01	0.007	0.007	0.001	0.001
4 min	0.05	0.005	0.002	0.002	0.0003	0.0002
5 min	0.02	0.002	0.001	0.0007	0.0001	9.14E-5

Table 4.25: Concentration ($\mu\text{g}/\text{m}^3$) Versus Time for JP-4 at 20°C

Time	A-B, Cont	B-C, Cont	C-D, Cont	A-B, Inst	B-C, Inst	C-D, Inst
1 sec	40247	3806	2084	36862	5570	4857
2 sec	7681	726	398	3786	572	499
3 sec	2752	260	143	944	143	124
4 sec	1244	118	64.4	330	49.9	43.5
5 sec	700	66.2	36.2	152	23.0	20.0
10 sec	98.7	9.34	5.11	11.5	1.74	1.52
20 sec	14.0	1.33	0.73	0.88	0.13	0.12
30 sec	4.40	0.33	0.18	0.15	0.02	0.02
40 sec	1.03	0.10	0.05	0.03	0.005	0.005
50 sec	0.34	0.03	0.02	0.009	0.001	0.001
1 min	0.12	0.01	0.006	0.003	0.0004	0.0004

Table 4.26: Concentration ($\mu\text{g}/\text{m}^3$) Versus Time for JP-8 at -20°C

Time	A-B, Cont	B-C, Cont	C-D, Cont	A-B, Inst	B-C, Inst	C-D, Inst
1 sec	216098	20435	11192	12863794	1943713	1694986
2 sec	61119	5780	3165	1957837	295828	257973
3 sec	29121	2754	1508	649208	98095	85542
4 sec	17027	1610	882	293512	44349	38674
5 sec	10718	1014	555	151337	22867	19941
10 sec	2955	279	153	22450	3392	2958
20 sec	710	67.1	36.8	2903	439	382
30 sec	279	26.3	14.4	793	120	104
40 sec	137	13.0	7.12	302	45.7	40.0
50 sec	87.0	8.23	4.51	157	23.7	20.7
1 min	47.5	4.49	2.46	72.8	11.0	9.59
2 min	6.88	0.65	0.36	5.67	0.86	0.75
3 min	2.59	0.24	0.13	1.48	0.22	0.20
4 min	1.36	0.13	0.07	0.60	0.09	0.08
5 min	0.29	0.03	0.02	0.11	0.02	0.01

Table 4.27: Concentration ($\mu\text{g}/\text{m}^3$) Versus Time for JP-8 at 0°C

Time	A-B, Cont	B-C, Cont	C-D, Cont	A-B, Inst	B-C, Inst	C-D, Inst
1 sec	195517	18489	10125	4764099	719853	627737
2 sec	52643	4978	2727	690271	104300	90953
3 sec	23894	2259	1237	218038	32945	28730
4 sec	13633	1289	706	96197	14535	12675
5 sec	8530	807	442	49305	7450	6497
10 sec	2023	191	105	6292	951	829
20 sec	401	38.0	20.8	672	101	88.5
30 sec	148	14.0	7.66	172	26.0	22.7
40 sec	66.2	6.26	3.43	59.7	9.01	7.86
50 sec	30.0	2.83	1.55	22.1	3.34	2.91
1 min	18.6	1.76	0.96	11.7	1.76	1.54
2 min	2.21	0.21	0.11	0.74	0.11	0.10
3 min	0.40	0.04	0.02	0.09	0.01	0.01
4 min	0.19	0.02	0.01	0.03	0.005	0.004
5 min	0.08	0.008	0.004	0.01	0.002	0.002

Table 4.28: Concentration ($\mu\text{g}/\text{m}^3$) Versus Time for JP-8 at 20°C

Time	A-B, Cont	B-C, Cont	C-D, Cont	A-B, Inst	B-C, Inst	C-D, Inst
1 sec	152755	14445	7911	998534	150878	131571
2 sec	36950	3494	1914	129975	19639	17126
3 sec	15395	1456	797	37687	5694	4966
4 sec	8284	783	429	15680	2369	2066
5 sec	4876	461	253	7561	1142	996
10 sec	935	88.4	48.4	780	118	103
20 sec	140	13.3	7.26	63.0	9.52	8.30
30 sec	34.0	3.21	1.76	10.6	1.60	1.40
40 sec	10.3	0.97	0.53	2.49	0.38	0.33
50 sec	3.35	0.32	0.17	0.66	0.10	0.09
1 min	1.21	0.11	0.06	0.20	0.03	0.03

Tables 4.23 through 4.28 give the three temperature conditions for both the continuous (Cont) and Instantaneous (Inst) cases. We see that concentrations fall below the hydrocarbon standard of $160 \mu\text{g}/\text{m}^3$ (defined as "critical") in a relatively short period of time for all cases, although the A-B case is more time critical (while the other cases are experiencing more dispersion with time due to higher ground wind velocities); moreover, depending on which fuel is used as well as the outside temperature, we see a considerable range in concentration versus time for all the conditions.

Finally, we see a comparison of critical times and distances for the three stability classes (A-B, B-C, C-D) with Tables 4.29 and 4.30 (which show the time and distance it takes to fall under the standard of $160 \mu\text{g}/\text{m}^3$):

Table 4.29: Critical Time and Distances for Various Conditions, Cont Case

Fuel/Temp	Condition	Time/Dist	Condition	Time/Dist	Condition	Time/Dist
JP-4/-20C	A-B	20.8 / 20.8	B-C	9.0 / 27.0	C-D	7.1 / 35.4
JP-4/ 0C	A-B	17.3 / 17.3	B-C	6.1 / 18.3	C-D	4.3 / 21.7
JP-4/ 20C	A-B	9.5 / 9.5	B-C	3.7 / 11.1	C-D	2.9 / 14.7
JP-8/-20C	A-B	38.4 / 38.4	B-C	15.6 / 46.8	C-D	9.9 / 49.6
JP-8/ 0C	A-B	29.5 / 29.5	B-C	12.0 / 36.1	C-D	9.2 / 45.9
JP-8/ 20C	A-B	19.7 / 19.7	B-C	9.0 / 27.1	C-D	7.3 / 36.4

Table 4.30: Critical Time and Distances for Various Conditions, Inst Case

Fuel/Temp	Condition	Time/Dist	Condition	Time/Dist	Condition	Time/Dist
JP-4/-20C	A-B	19.9 / 19.9	B-C	13.8 / 41.3	C-D	12.7 / 63.5
JP-4/ 0C	A-B	14.0 / 14.0	B-C	8.1 / 24.4	C-D	7.8 / 38.9
JP-4/ 20C	A-B	5.0 / 5.0	B-C	3.0 / 8.9	C-D	2.9 / 14.5
JP-8/-20C	A-B	49.8 / 49.8	B-C	28.7 / 86.2	C-D	28.0 / 139.9
JP-8/ 0C	A-B	31.1 / 31.1	B-C	19.3 / 57.9	C-D	19.0 / 95.2
JP-8/ 20C	A-B	18.6 / 18.6	B-C	9.8 / 29.4	C-D	9.7 / 48.4

We observe a trend of increasing critical distances (for both the continuous case and instantaneous case) as we move from A-B to C-D (unstable to neutral) because of the move to more stable atmospheric conditions. In other words, the concentrations do not drop below the standard until further distances downwind as the stability classes go from unstable (A-B) to neutral (C-D) conditions. However, we observe the opposite effect for time; time critical conditions go in decreasing order from A-B to C-D (while distance critical conditions go in increasing order from A-B to C-D) because the increasing ground wind velocities from A-B to C-D create more aerosol dispersion. Again, we observe that when the aerosol is JP-8, it is at higher concentrations than its JP-4 counterpart at the same conditions. We also observe that lower temperatures yield less evaporation and therefore higher aerosol concentrations than higher temperatures.

4.6 Summary of Results.

The results presented in this chapter show the general findings of Clewell and apply them to our specific problem. We see a range of 1.16 to 12.3% making it to the ground for -20°C to 20°C (JP-4), and a range of 11.2 to 52.6% for JP-8. Advection and dispersion works with evaporation to decrease the airborne concentration with time of our

aerosol. Perhaps time is irrelevant for the continuous case, since what we are concerned with is the distance it takes to go below the standard while the fuel is continuously being emitted until combustion occurs. For the instantaneous case, however, time to go below the standard (as well as distance) is indeed important. Therefore, as we quantify downwind concentrations with time and distance, we are able to quantify the critical time and distances for various conditions. Tables 4.29 and 4.30 show that the most critical distance case for the instantaneous condition is **140 meters**, which corresponds to the C-D case, JP-8, and -20°C. The most critical time case for the instantaneous condition is **50 seconds**, which corresponds to the A-B case, JP-8, and -20°C.

For the continuous case, the distance critical case is **50 meters**, corresponding to the C-D case, JP-8, and -20°C. The time critical case is **38.4 seconds** (A-B case, JP-8, -20°C), although if we assume a cold startup process of 10 minutes, this time critical case is of little significance because we will be concerned with high aerosol concentrations close to the source for this entire cold startup period.

V. Summary and Conclusions.

5.1 Summary.

5.1.1 Aerosol Settling. It was observed that 92% of our aerosol mass is included in the 5 to 100 μm range, with approximately 60% of the aerosol mass in the 5 to 60 μm range. Hence, with this mass concentration towards the lower end of the range, the majority of the aerosol mass takes between 1 and 10 minutes to settle to the ground from our source height of 3 meters. Of course, evaporation acts to increase the settling times because of the decrease in the droplet size.

5.1.2 Aerosol Advection and Dispersion. With the three atmospheric conditions simulated (from unstable to neutral), a considerable range of airborne concentrations with time was observed. Of interest was the effect of either wind velocity or atmospheric stability on the aerosol concentrations; the unstable case (A-B) was more time critical due to the slower wind velocity (1 m/s) while the neutral case (C-D) was more distance critical due to less atmospheric dispersion (more atmospherically stable).

5.1.3 Aerosol Evaporation. Evaporation significantly impacted the aerosol concentration with time as it was observed the airborne aerosol to evaporate relatively quickly (within 5 minutes). Temperature was found to be the controlling physical factor as we observed a sizable range in total JP-8 evaporation (42% from -20°C to 20°C), and a comparatively modest range in JP-4 evaporation (11% from -20°C to 20°C). Of course, due to its greater volatility, JP-4 evaporates more quickly than JP-8 (25% average difference for the three temperatures). For JP-8, 53%, 28%, and 11% of the aerosol made

ground-fall for -20°C , 0°C and 20°C , respectively. For JP-4, 12%, 4%, and 1%, respectively, made ground-fall.

5.2 Conclusions.

Because the purpose of this thesis was to elucidate a problem at northern tier bases, the conclusions to be drawn from this study may be helpful in focusing further studies in this area; however, the results should not to be used to make conclusions regarding long-term health effects because of the underlying assumptions used in this study.

With the airborne concentrations, potential long-term health problems may very well exist as we observed extremely high aerosol concentrations close to the source for our B-52H case (while the B-52G and B-1 were not as significant, see Table 4.9). Moreover, the continuous plume case gives aerosol concentrations in excess of the hydrocarbon standard up to 50 meters downwind of the source (for the most critical case), while the instantaneous source gives aerosol concentrations in excess of the standard up to 140 meters downwind of the source, lasting as long as 50 seconds. In addition, the constituent data gives an idea of the chemical make-up of the ingested aerosol at different times.

With the ground concentrations, potential threats to the groundwater may be of concern depending on the temperature and fuel type. For the -20°C JP-8 case, 53% reaches the ground, proving to be significant compared to 1% for the 20°C , JP-4 case.

5.3 Recommendations.

With future studies, it may be worthwhile to investigate more closely the actual emitted particle size distribution; this study focused on aerosol theory versus what

actually takes place on the flight-line. Moreover, since we assumed laminar flow in the advection and dispersion calculations (we assumed atmospheric conditions and wind take over after emission), it would be worthwhile to investigate the effect of turbulent motion close to the source. In general, however, due to the theoretical nature of this study, future follow-on work in this area should be more empirical in nature, possibly measuring actual airborne and ground concentrations of the aerosol as it is being emitted.

As was mentioned in the introduction, the cold startup time was assumed to be 10 minutes to simplify the study; the effects of temperature on the cold startup time may be worthwhile to study. In addition, since hydrocarbon vapor was neglected in this study, it would indeed be worthwhile to determine downwind hydrocarbon vapor concentrations as a result of cold startup. The vapor concentrations should be taken into account with the aerosol concentrations to determine overall long term inhalation health effects. Finally, it may be worthwhile to examine the effects of coagulation and condensation, if any, on our aerosol (since it was assumed that our particle size distribution would be constant with time).

Appendix A. Evaporation Model

This is the evaporation model based on the work of Clewell (4). This Fortran model, used with the fuel information in Appendix B, yields our evaporation results. The model requires the following data input: the ambient air temperature ($^{\circ}\text{C}$), the droplet size (μm), the droplet initial velocity (m/s), and the height of aerosol emission (m).

```

program main
integer neq,nparam
parameter (neq=9,nparam=50)
integer ido,imeth,inorm
real a(1,1),fcn,fcnj,hinit,param(nparam),tol,t,tend,c(neq)
real al(12),pcv(33),mw(33),bpt(33),dens(33),vc(33)
real mi,m(33),molf(33),mrel,mr(33),msave(33),md,moles,mrel
real mev(33),mstep,nuh,num,ms
external fcn,fcnj,ivpag
c this program must be run with the command f77-1.4 file.f -limsl
c to print this file, type 'enscript -h -Prm1 14hp4p file.f
c page numbers refer to pages in ESL-TR-80-56 by Clewell
read 992, tg,dmic,v,hi
992 format(1x,3f4.0,f7.0)
ncomp=27
c read fuel composition data
do 5 i=1,2
read 998, (al(j),j=1,12)
5 continue
do 10 i=1,ncomp
read 997, (al(j),j=1,6),pcv(i),mw(i),bpt(i),dens(i)
print 996, (al(j),j=1,6),pcv(i),mw(i),bpt(i),dens(i)
dcfb=1./(1+.001*(bpt(i)-293.15))
vc(i)=mw(i)/(dens(i)*dcfb)
10 continue
c initial conditions
nmax=100
ipmax=100
iprn=0
dhmax=100.
dmmax=.05
alb=.14
ea=.75
ed=.95
rs=1000.
hg=0.
print 994, tg,dmic,v,hi
t0=tg+.0065*hg+273.15
137 di=.000001*dmic
d=di
h=hi
ut=0.
t=0.
idone=0
tstep=1.

```

```

      npas=1
c   see page 87, dt is delta temp for initial temperature calculation
      ta=t0-.0065*h
      cs=20.*sqrt(ta)
      dtsav=-ta*v*v/cs/cs/5.
      dt=dtsav
      ids=0
c   beginning calculation loop
c   see page 86, calculate ambient conditions
140 ta=t0-.0065*h
      pa=101315.*(ta/t0)**5.256
      densa=.003484*pa/ta
      visca=1.458e-6/(110.4+ta)*ta**1.5
c   see page 87
      td=ta-dt
      tf=.5*(ta+td)
      dcfld=1./(1.+0.001*(td-293.15))
c   on initial pass, calculate droplet volume and mass
      if(npas.gt.1) go to 160
      vd=.5236*d**3
      mi=0.
      do 150 i=1,ncomp
      m(i)=dens(i)*dcfld*pcv(i)*vd
      msave(i)=m(i)
150 mi=mi+m(i)
      md=mi
      densi=md/vd
c   calculate composition and size of droplet
160 moles=0.
      do 170 i=1,ncomp
170 moles=moles+m(i)/mw(i)
      vd=0.
      do 180 i=1, ncomp
180 vd=vd+m(i)/(dens(i)*dcfld)
c   vol=(4/3)pi r cubed = (pi/6) d cubed, so d = (1.90986 vol)**(1/3)
      d=(1.90986*vd)**(1./3.)
      dmic=1000000.*d
c   molf is epsilon sub i on page 88
      do 185 i=1,ncomp
185 molf(i)=m(i)/(mw(i)*moles)
      densd=md/vd
186 mrel=md/mi
      do 190 i=1,ncomp
190 mr(i)=m(i)/msave(i)
c   single droplet printout

```

```

tt=t/60.
print 995, npas,ids
print 994,dt,td,dcfd,vd,tstep
995 format(1x,2i5)
218 print 994, tt,h,dmic,ut,mrel
994 format(1x,5e14.5)
iprn=iprn+1
if(npas.ge.nmax) stop
if(idone.ge.1) stop
980 format(1x,f7.3,4x,f6.0,7x,f5.0,7x,f6.4,6x,f6.4,4x,9(2x,f4.2))
c calculate free fall and evaporation, see page 87
220 q=sqrt((4.*densa*densd*9.8*d**3)/3.)/visca
qln=alog(q)
c see page 88, reynolds number
rey=exp(-3.13+2.06*qln-.083*qln*qln)
ut=visca*rey/(d*densa)
hstep=ut*tstep
c see page 92, dify is D sub i, num is Nu sub i, hm is h sub i
mstep=0.
do 225 i=1,ncomp
dify=2.66E-5*sqrt(1./mw(i)+.0345)*tf*tf/
1(pa*(vc(i)**(1./3.))+.31)**2)
num=2.+6*sqrt(rey)*(visca/(densa*dify))**(1./3.)
hm=num*dify*mw(i)/(8314.34*d*ta)
c see page 90, pv is component vapor pressure
arg=(20.53-2899./(385.15*td/bpt(i)-62.3))
if(arg.gt.20.) arg=20.
pv=exp(arg)
c see page 88, mev is component mass evaporated
c mstep is the total mass evaporated
mev(i)=3.14159265*d*d*hm*pv*molf(i)*tstep
ms=mev(i)
if(ms.gt.m(i)) ms=m(i)
if(arg.gt.19.) print 994,arg,pv,mev(i)
225 mstep=mstep+ms
npas=npas+1
if(npas.le.nmax) go to 230
if(npas.ge.nmax) stop
c skip heat balance if calculating droplet cooling
230 if(ids.eq.1) go to 234
c calculate steady-state temperature differences
oldt=dt
tka=.024+8.1e-5*(ta-273.15)
pr=.713-3.3e-4*(ta-273.15)
nuh=2.+6*sqrt(rey)*pr**(1./3.)

```



```

      hh=tka*nuh/d
      dhvap=3.7e5*(1.-.0013*(td-273.15))
231 dtnw=5.67e-8*ea*ta**4-5.67e-8*ed*td**4+.25*(1.-alb)*rs+hh*dt
      1-dhvap*mstep/(3.14159*d*d*tstep)
      td=td+dtlw/(hh+2.27e-7*ed*td**3)
      if(abs(ta-dt-td).le..1) go to 232
      dt=ta-td
      go to 231
232 if(abs(ta-td-oldt).le..5) go to 234
      dt=(ta-td+oldt)/2.
      go to 140
234 dt=ta-td
c skip droplet cooling after steady-state temperature is reached
      if(ids.eq.2) go to 240
      if(ids.eq.1) go to 238
      if(dt.gt.dtsav) go to 236
c   set indicator that droplet cooling is no longer needed
      ids=2
      go to 240
c   restore dt and set indicator to calculate droplet cooling
236 ids=1
      dt=dtsav
      go to 140
c   calculate droplet cooling and reset indicator to heat balance
238 ids=0
      cp=4184.*(181.+8*td)*vd
      dhvap=3.7e5*(1.-.0013*(td-273.15))
      dcool=(ea*5.67e-8*ta**4-ed*5.67e-8*td**4+.25*(1.-alb)*rs
      1+tka*nuh*dtsav/d)*3.14159*d*d*tstep
      dcool=(dcool-mstep*dhvap)/cp
      print 994,dcool
      dclmn=dtsave+100.-ta
      if(dcool.lt.dclmn) dcool=dclmn
      dtsav=dtsav-dcool
      dcsav=dcool
      dt=dtsav
c   halve increment until within limits
240 if(hstep.gt.dhmax) go to 250
      if(mstep/mi.le.dmmx) go to 275
250 tstep=tstep/2.
      hstep=hstep/2.
      mstep=0.
      do 260 i=1,ncomp
      mev(i)=mev(i)/2.
      ms=mev(i)

```

```

    if(ms.gt.m(i)) ms=m(i)
260 mstep=mstep+ms
    if(ids.eq.2) go to 240
    dcsav=dcav/2.
    dtsav=dtsav+dcsav
    dt=dtsav
    go to 240
c    update variables with results for increment
275 hs=h
    h=h-hstep
    if(h.lt.hg) go to 310
    t=t+tstep
    md=md-mstep
    do 280 i=1,ncomp
        if(mev(i).gt.m(i)) mev(i)=m(i)
280 m(i)=m(i)-mev(i)
c    increase duration of next increment
    tstep=2.*tstep
    if(md/mi.ge. .0005) go to 285
    idone=3
    go to 140
285 if(hstep.lt.10.) go to 290
    if(mstep/mi.lt. .005) go to 290
    go to 140
290 tstep=2.*tstep
    go to 140
c    end of calculation loop
310 print 993
993 format(1x,'evaporation has stopped')
    hinit=1.0e-3
    imeth=2
    h=.000001
    do 850 i=1,50
850 param(i)=0.
    param(1)=hinit
    param(4)=100000.
    param(12)=imeth
    ido=1
    do 860 i=1,neq
        x=float(i)/float(neq+1)
        pi=3.14159265
860 c(i)=sin(pi*x)
    print 999,(c(i),i=1,neq)
    t=0.
    tol=1.0e-6

```

```

npp=2
do 870 kk=1,npp
tend=.01*float(kk)/float(npp)
call ivpag(ido,neq,fcn,fcnj,a,t,tend,tol,param,c)
print 999,t,(c(i),i=1,neq)
999 format(1x,5e14.5)
870 continue
ido=3
call ivpag(ido,neq,fcn,fcnj,a,t,tend,tol,param,c)
998 format(12a6)
997 format(5a6,a2,f5.0,1x,f5.0,1x,f6.0,1x,f5.0)
996 format(1x,5a6,a2,1x,f5.3,1x,f6.2,1x,f6.2,1x,f5.0)
stop
end
subroutine fcn(neq,t,c,dc)
integer neq
real t,c(neq),dc(neq)
d=1.
rskdon=.0239
csfc=2497.
thick=1.
delx=thick/float(neq+1)
dxsq=delx*delx
cz=rskdon*csfc
cz=0.
dc(1)=d*(c(2)-2.*c(1)+cz)/dxsq
nm1=neq-1
do 100 i=2,nm1
100 dc(i)=d*(c(i+1)-2.*c(i)+c(i-1))/dxsq
dc(neq)=0.
dc(neq)=d*(c(neq-1)-2.*c(neq))/dxsq
RETURN
END
SUBROUTINE FCNJ(N,T,F,PD)
integer n
real t,f(n),pd(*)
RETURN
END

```

Appendix B. Clewell's Fuel Component Models

In establishing our evaporation model, we use the multi-component fuel models developed by Clewell. Units were converted from original model (4:5-6) for ease in our model calculations.

CLEWELL'S 33-COMPONENT SYNTHETIC JP-4 and 27-COMPONENT JP-8

Composition data format is:

label;

volume percent;

molecular weight (in kg/kmol);

boiling point at standard temperature and pressure (in K);

density (in kg/m³)

NOTE: Original table (Clewell) gave reference densities in g/ml. Have converted these to kg/m³ to be consistent with model computations.

NOTE: Original table (Clewell) gave volume_percent. Have changed this to volume fraction so that we do not have to divide by 100 every time we use this number.

NOTE: Original table (Clewell) gave boiling points in Celsius. All computations need Kelvin. Have adjusted entries to Kelvin (using $K = C + 273.15$).

a) fuel_type=JP-4 (Clewell)

number_of_components=33

component=C5 hydrocarbons; 0.039; 72.20;301.05;620.0

component=C6 paraffins; 0.081; 86.20;333.35;660.0

component=C6 cycloparaffins; 0.021; 84.20;353.85;780.0

component=Benzene; 0.003; 78.10;353.25;880.0

component=C7 paraffins; 0.094;100.20;364.95;690.0

component=C7 cycloparaffins; 0.071; 98.20;374.05;770.0

component=Toluene; 0.007; 92.10;383.95;870.0

component=C8 paraffins; 0.101;114.20;390.85;700.0

component=C8 cycloparaffins; 0.074;112.20;397.45;780.0

component=C8 aromatics; 0.016;106.20;412.25;870.0

component=C9 paraffins; 0.091;128.30;415.55;720.0

component=C9 cycloparaffins; 0.043;126.20;427.65;800.0

component=C9 aromatics; 0.024;120.20;438.35;880.0

component=C10 paraffins; 0.073;142.30;432.75;720.0

component=C10 cycloparaffins; 0.037;140.30;444.05;800.0

component=C10 aromatics; 0.018;134.20;450.25;860.0

component=Napthalene; 0.002;128.20;491.05;1030.0

component=C11 paraffins; 0.048;156.30;469.05;740.0

component=C11 cycloparaffins; 0.025;154.30;469.65;800.0

component=Dicycloparaffins; 0.034;150.30;474.15;890.0

component=C11 aromatics; 0.011;148.20;478.15;860.0
 component=C11 naphthalenes; 0.002;142.20;517.75;1020.0
 component=C12 paraffins; 0.028;170.30;489.45;750.0
 component=C12 cycloparaffins; 0.012;168.30;484.15;800.0
 component=C12 aromatics; 0.005;162.30;489.15;860.0
 component=C12 naphthalenes; 0.002;156.20;541.15;1000.0
 component=C13 paraffins; 0.011;184.40;508.55;760.0
 component=C13 cycloparaffins; 0.004;182.40;498.15;800.0
 component=C13 aromatics; 0.001;176.30;507.15;870.0
 component=C14 hydrocarbons; 0.002;198.40;526.85;760.0
 component=C15 hydrocarbons; 0.001;212.40;543.75;770.0
 component=Tricycloparaffins; 0.018;192.40;563.15;940.0
 component=Residual hydrocarbons;0.001;202.30;666.15;1270.0

b) fuel_type=JP-8 (Clewell)

number_of_components=27

component=C8 paraffins; 0.003;114.2;391.15; 700.0
 component=C8 cycloparaffins; 0.002;112.2;397.15; 780.0
 component=C8 aromatics; 0.001;106.2;412.15; 870.0
 component=C9 paraffins; 0.024;128.3;415.15; 720.0
 component=C9 cycloparaffins; 0.015;126.2;427.15; 800.0
 component=C9 aromatics; 0.010;120.2;438.15; 880.0

component=C10 paraffins; 0.056;142.3;433.15; 720.0
component=C10 cycloparaffins; 0.035;140.3;444.15; 800.0
component=C10 aromatics; 0.023;134.2;450.15; 860.0
component=C11 paraffins; 0.087;156.3;469.15; 740.0
component=C11 cycloparaffins; 0.033;154.3;469.15; 800.0
component=Dicycloparaffins; 0.031;152.3;474.15; 890.0
component=C11 aromatics; 0.036;148.2;478.15; 860.0
component=C12 paraffins; 0.108;170.3;489.15; 750.0
component=C12 cycloparaffins; 0.080;166.3;494.15; 880.0
component=C12 aromatics; 0.046;162.3;489.15; 860.0
component=C13 paraffins; 0.115;184.4;508.15; 760.0
component=C13 cycloparaffins; 0.085;182.4;498.15; 800.0
component=C13 aromatics; 0.049;176.3;507.15; 870.0
component=C14 paraffins; 0.059;198.4;527.15; 760.0
component=C14 cycloparaffins; 0.044;192.4;563.15; 940.0
component=C14 aromatics; 0.025;186.3;568.15;1030.0
component=C15 paraffins; 0.014;212.4;544.15; 770.0
component=C15 cycloparaffins; 0.010;206.4;573.15; 900.0
component=C15 aromatics; 0.006;200.4;578.15; 950.0
component=C16 hydrocarbons; 0.002;226.4;560.15; 770.0
component=Residual hydrocarbons;0.001;202.3;666.15;1270.0

Bibliography

1. Bird, R. Byron, et al. *Transport Phenomena*, New York: John Wiley and Sons, 1960.
2. Bolin, B., et al. "Residence Time of Atmospheric Pollutants as Dependent on Source Characteristics, Atmospheric Diffusion Processes, and Sink Mechanisms," *Tellus*, 26, pgs. 185-194, 1974.
3. Brock, J.R. "Condensational Growth of Atmospheric Aerosols," *Journal of Colloid Interface Science*, 39, pgs. 32-36, 1972.
4. Clewell, Harvey J. III, "Evaporation and Groundfall of JP-4 Jet Fuel Jettisoned by USAF Aircraft," Engineering and Services Laboratory, Air Force Engineering and Services Center (AFESC), 1980.
5. Clewell, Harvey J. III, "Ground Contamination by Fuel Jettisoned from Aircraft in Flight," *Journal of Aircraft*, 20 (4), pgs. 382-384, 1983.
6. Dana, M. Terry, and Hales, Jeremy M., "Statistical Aspects of the Washout of Polydisperse Aerosols," *Atmospheric Environment*, 10, pgs. 45-50, 1976.
7. Davies, C.N., *Recent Advances in Aerosol Research*, The Macmillan Company, N.Y.: 1964.
8. Finlayson-Pitts, Barbara J., and Pitts, James N., *Atmospheric Chemistry: Fundamentals and Experimental Techniques*, John Wiley & Sons, N.Y.: 1986.
9. Friedlander, S.K., *Smoke, Dust and Haze: Fundamentals of Aerosol Behavior*, John Wiley & Sons, N.Y.: 1977.
10. Fuchs, N.A., *The Mechanics of Aerosols*, The Macmillan Company, N.Y.: 1964.
11. Gelbard, Fred, and Seinfeld, John H., "Exact Solution of the General Dynamic Equation for Aerosol Growth by Condensation," *Journal of Colloid Interface Science*, 68, pgs. 173-183, 1979.
12. Good, R. Earl, and Clewell, Harvey J., "Drop Formation and Evaporation of JP-4 Fuel Jettisoned from Aircraft," *Journal of Aircraft*, 17 (7), pgs. 450-456, 1980.
13. Grover, S.N., et al. "A Numerical Determination of the Efficiency with Which Spherical Aerosol Particles Collide with Spherical Water Drops Due to Inertial Impaction and Phoretic and Electrical Forces," *Journal of Atmospheric Science*, 34, pgs. 1655-1663, 1977.

14. Heiklen, Julian, "Atmospheric Lifetimes of Pollutants," *Atmospheric Environment*, 16, pgs. 821-823, 1982.
15. Hinze, J.O., "Critical Speeds and Sizes of Liquid Globules," *Applied Science Research*, Hague A, Vol. I, pgs. 273-288, 1949.
16. Hobbs, Peter V., *Aerosol-Cloud-Climate Interactions*, Academic Press, CA.: 1993.
17. Lowell, Herman H., "Free Fall and Evaporation of JP-4 Jet Fuel Droplets in a Quiet Atmosphere," Technical Note, NASA TN D-33, 1959.
18. Lowell, Herman H., "Dispersion of Jettisoned JP-4 Jet Fuel by Atmospheric Turbulence, Evaporation, and Varying Rates of Fall of Fuel Droplets," Technical Note, NASA TN D-84, 1959.
19. Marlow, William H., "Size Effects in Aerosol Particle Interactions: The Van Der Waals Potential and Collision Rates," *Surface Science*, 106, pgs. 529-537, 1981.
20. Pfeiffer, Karl D., "A Numerical Model to Predict the Fate of Jettisoned Aviation Fuel," MS Thesis, Air Force Institute of Technology, Wright-Patterson Air Force Base, 1994.
21. Pfeiffer, Karl D., Quinn, Dennis W., and Dungey, Clifton E., "Numerical Model to Predict the Fate of Jettisoned Aviation Fuel," *Journal of Aircraft*, 33 (2), pgs. 353-362, 1996.
22. Quackenbush, Todd R., et al. "A Model for Assessing Fuel Jettisoning Effects," *Atmospheric Environment*, 28 (16), pgs. 2751-2759, 1994.
23. Ramabhadran, T.E., et al. "Dynamics of Aerosol Coagulation and Condensation," *AIChE Journal*, 22, pgs. 840-851, 1976.
24. Seinfeld, John H., *Atmospheric Chemistry and Physics of Air Pollution*. John Wiley and Sons, N.Y.: 1986.
25. Slinn, W.G.N., "Relationships Between Removal Processes and Residence Times for Atmospheric Pollutants," *AIChE Symposium Series*, #196, Vol. 76, pgs. 185-203, 1980.
26. Sundqvist, H., et al. "Condensation and Cloud Parameterization Studies with a Mesoscale Numerical Weather Prediction Model," *Monthly Weather Review*, 117, pgs. 1641-1657, 1989.

27. Todd, Jeffrey M., "An Assessment of the Impact of Fuel Jettisoning Events Using Simulation and Impact Models," MS Thesis, Air Force Institute of Technology, Wright-Patterson Air Force Base, 1995.
28. Turner, Bruce D., *Workbook of Atmospheric Dispersion Estimates*, U.S. Department of Health, Education, and Welfare, Cincinnati, Ohio, 1969.
29. Wark, Kenneth, and Warner, Cecil F., *Air Pollution: Its Origin and Control*, Harper Collins Publishers, N.Y., 1981.
30. Wesely, M.L., et al. "An Eddy Correlation Measurement of Particulate Deposition from the Atmosphere," *Atmospheric Environment*, 11, pgs. 561-563, 1977.
31. Willeke, Klaus, and Baron, Paul A., *Aerosol Measurement: Principles, Techniques and Applications*, Van Nostrand Reinhold, N.Y., 1993.
32. Williams, M.M.R., "On Some Exact Solutions of the Space and Time Dependent Coagulation Equation for Aerosols," *Journal of Colloid Interface Science*, 101, pgs. 19-26, 1984.
33. Williams, M.M.R., and Loyalka, Sudarshan K., *Aerosol Science: Theory and Practice*, Pergamon Press, N.Y., 1991.

Vita

Capt Buckman was born [REDACTED]. He attended the University of Washington in Seattle, Washington and graduated with a Bachelor of Science in Civil Engineering in 1993.

Capt Buckman spent three years at McChord AFB, Tacoma, WA, where he served in the 62 Civil Engineer Squadron. During the three years, he spent one year as a Civil Designer and two years as a Base Programmer. He was deployed to Riyadh, Saudi Arabia for three months during December, 1995 to March, 1996, where he served as the Environmental Engineer. In March, 1996, he was selected to attend AFIT in residence at Wright Patterson Air Force Base, Dayton, Ohio for completion of a Master of Science in Environmental Engineering and Management.

Permanent address: [REDACTED]

REPORT DOCUMENTATION PAGE			Form Approved OMB No. 0704-0188	
<small>Public reporting burden for this collection of information is estimated to average 1 hour per response, including the time for reviewing instructions, searching existing data sources, gathering and maintaining the data needed, and completing and reviewing the collection of information. Send comments regarding this burden estimate or any other aspect of this collection of information, including suggestions for reducing this burden, to Washington Headquarters Services, Directorate for Information Operations and Reports, 1215 Jefferson Davis Highway, Suite 1204, Arlington, VA 22202-4302, and to the Office of Management and Budget, Paperwork Reduction Project (0704-0188), Washington, DC 20503.</small>				
1. AGENCY USE ONLY (Leave blank)		2. REPORT DATE December 1997		3. REPORT TYPE AND DATES COVERED Final
4. TITLE AND SUBTITLE The Fate and Transport of Airborne JP-4 and JP-8 Aerosol During Cold Startup			5. FUNDING NUMBERS	
6. AUTHOR(S) Captain Bradford E. Buckman				
7. PERFORMING ORGANIZATION NAME(S) AND ADDRESS(ES) Air Force Institute of Technology 2750 P Street WPAFB OH 45433-7765			8. PERFORMING ORGANIZATION REPORT NUMBER AFIT/GEE/ENC/97D-02	
9. SPONSORING/MONITORING AGENCY NAME(S) AND ADDRESS(ES) Air Force Office of Scientific Research 110 Duncan Avenue, Suite B115 Bolling AFB, DC 20332-0001			10. SPONSORING/MONITORING AGENCY REPORT NUMBER	
11. SUPPLEMENTARY NOTES				
12a. DISTRIBUTION AVAILABILITY STATEMENT Approved for public release; distribution unlimited			12b. DISTRIBUTION CODE	
13. ABSTRACT (Maximum 200 words) <p>During cold startup (engine warm-up) procedures at northern tier bases, fuel aerosol (JP-4 and JP-8) is emitted before complete combustion of the fuel occurs. The time necessary for complete combustion to occur may be as long as ten minutes. Hence, during these first few minutes, aerosol is emitted at relatively high concentrations.</p> <p>This research investigates the principle behavior of the emitted aerosol: advection, dispersion, evaporation, and settling. Using previous work in fuel jettisoning and evaporation as a foundation, this thesis investigates the physical factors affecting the airborne concentration of fuel aerosol at different times, the amount of fuel aerosol reaching the ground, and the times and distances necessary for the aerosol concentration to fall below the hydrocarbon standard after being emitted. Physical assumptions in the model are presented, limitations of the assumptions discussed, and various atmospheric conditions are simulated for comparison.</p>				
14. SUBJECT TERMS			15. NUMBER OF PAGES 80	
			16. PRICE CODE	
17. SECURITY CLASSIFICATION OF REPORT Unclassified	18. SECURITY CLASSIFICATION OF THIS PAGE Unclassified	19. SECURITY CLASSIFICATION OF ABSTRACT Unclassified	20. LIMITATION OF ABSTRACT UL	